



# Metal SLS – a new alternative for LPBF?

---

Alliance Deep Dive | 2023



— ADDITIVE —  
**ALLIANCE**

**exclusive**

## Contact

---

Fraunhofer Research Institution for  
Additive Manufacturing Technologies IAPT



Am Schleusengraben 14  
21029 Hamburg-Bergedorf  
Germany



+49 40 48 40 10-500



marketing@iapt.fraunhofer.de



[www.iapt.fraunhofer.de](http://www.iapt.fraunhofer.de)



[www.linkedin.com/company/fraunhofer-iapt](https://www.linkedin.com/company/fraunhofer-iapt)



[www.youtube.com/FraunhoferIAPT](https://www.youtube.com/FraunhoferIAPT)

# 1. Abstract

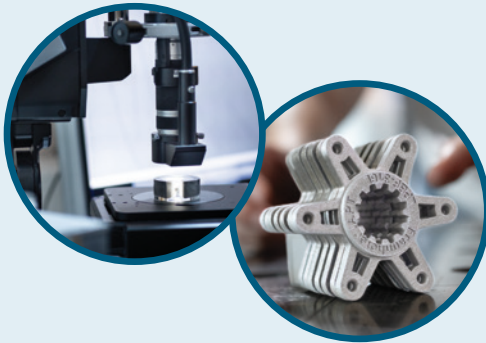
---

## Motivation



- Series production in LPBF hindered by supports:
  - Extra time
  - Extra costs
- Metal SLS = LPBF without supports

## Approach



- Investigation of the economic potential
- Investigation of part quality of Metal SLS and LPBF produced specimens

## Results



- Economical comparison
- Part quality comparison



## 2. Content

---

<b>1. Abstract</b>	<b>3</b>
<b>2. Content</b>	<b>5</b>
<b>3. Acknowledgement</b>	<b>6</b>
<b>4. About the authors</b>	<b>7</b>
<b>5. Motivation</b>	<b>8</b>
<b>6. Approach of the Deep Dive</b>	<b>10</b>
<b>7. Methodology</b>	<b>14</b>
<b>8. Economical comparison</b>	<b>16</b>
8.1 Base process: Metal SLS	19
8.2 Base process: LPBF	20
8.3 Productivity boost: Metal SLS	22
8.4 Productivity boost: LPBF	27
8.5 Economic evaluation	30
8.6 Material efficiency	31
<b>9. Quality comparison</b>	<b>32</b>
9.1 Dimensional accuracy	34
9.2 Density	36
9.3 Tensile properties	38
9.4 Vickers hardness	41
9.5 Surface roughness	42
<b>10. Summary &amp; Conclusion</b>	<b>44</b>
<b>11. References</b>	<b>46</b>
<b>12. Imprint</b>	<b>47</b>

### 3. Acknowledgement

---

Deep Dives are reports intended exclusively for the members of the Additive Alliance®. They provide the latest insights into the science behind Additive Manufacturing (AM). We extend our profound thanks to the members listed below. This Deep Dive could not have been created without their financial support.



## 4. About the authors

---

The authors of this Deep Dive are Lennart Waalkes and Lennard Hermans. Their aim is to advance the industrial implementation of sinter-based AM technologies.

Both authors have been active in the field of sinter-based 3D printing for several years and have conducted various research projects. Their goal with the Deep Dive was to provide a well-founded overview of the potentials and challenges for the sinter-based 3D printing process Metal Selective Laser Sintering (Metal SLS) as a cost-effective production alternative for the established Laser Powder Bed Fusion (LPBF) process.



*Dr. Lennart Waalkes  
Head of Sinter AM Team*



*Lennard Hermans, M.Sc.  
Sinter AM Team*

### Contact

---

Dr. Lennart Waalkes  
Head of Sinter AM Team  
Telephone +49 40 48 40 10-762  
[lennart.waalkes@iapt.fraunhofer.de](mailto:lennart.waalkes@iapt.fraunhofer.de)  
[www.iapt.fraunhofer.de](http://www.iapt.fraunhofer.de)

# 5. Motivation

---

## What is Metal SLS?

Metal SLS is a novel process in which polymer-coated metal powder is processed on widespread SLS systems known from Additive Manufacturing (AM) with polymers. In contrast to the established LPBF process, machine costs are generally lower and no build plate or support structures are necessary. Separation from the build plate and removal of support structures of the SLS-printed parts is therefore not necessary. This saves time and money, as the use of support structures is generally associated with increased material consumption.

However, in Metal SLS the printed part is initially present as a so-called green part, in which the metal powder is only bound in a polymer matrix. The latter must then be removed from the metal powder by a solvent-based and subsequent thermal debinding process. The remaining metal powder is then densified in a final sintering step to form a purely metallic parts with its final mechanical properties.

Debinding and sintering are already known from the established production process Metal Injection Molding (MIM). The existing MIM process technology for debinding and sintering can generally be used for Metal SLS.

Combined with cost-effective SLS printing process, this new sinter-based AM process promises great cost advantages in the series production of metal AM parts.

This Deep Dive will therefore investigate the question whether Metal SLS is a real alternative for the established L-PBF process in terms of series production. For this purpose, both AM processes will be compared with respect to economic (e.g. costs per unit) and quality (e.g. tensile properties) aspects on the basis of an industrial demonstrator application.

## Insights to be gained:

1. Basics of Metal SLS
2. Economic consideration of lot-size dependent production in Metal SLS and LPBF
3. Quality assessment of 316L parts manufactured with Metal SLS and LPBF
4. Comprehensive overview of the economic and quality comparison





**Metal SLS powder can be processed into a green part in conventional SLS machines.«**





**316L Metal SLS powder  
four times more  
expensive compared  
to LPBF powder. «**

## 6. Approach of the Deep Dive

### Powder

The Metal SLS powder was specifically developed for use in SLS systems, where polymers are commonly processed. Unlike LPBF prepared powder, which demands high requirements regarding sphericity and flowability, a broader spectrum of powder forms can be utilized.

In Metal SLS, non-spherical powders with a wide range of particle size distribution can be processed, since the flowability is ensured by the binder [Hea20]. This further allows the processing of reactive metals as well as metals with a low light absorption coefficient. Polymer encapsulation also reduces the potential for an exothermically triggered dust explosion.

However, with a particle size of  $< 120 \mu\text{m}$  and a powder grain that is not fully encapsulated, it is recommended to handle the powder according to the safety standards of metal.

Figure 1 shows the SEM image of the powder grain, which is largely covered with binder.

### SLS printing

At the beginning of Metal SLS, the loaded plastic powder is processed into green parts using commercially available polymer SLS equipment. Analogous to SLS with pure polymer powders, the Metal SLS powder is also fused by means of a laser. The SLS process begins with a thin layer of powdered material spread on a build platform. The laser scans the cross-

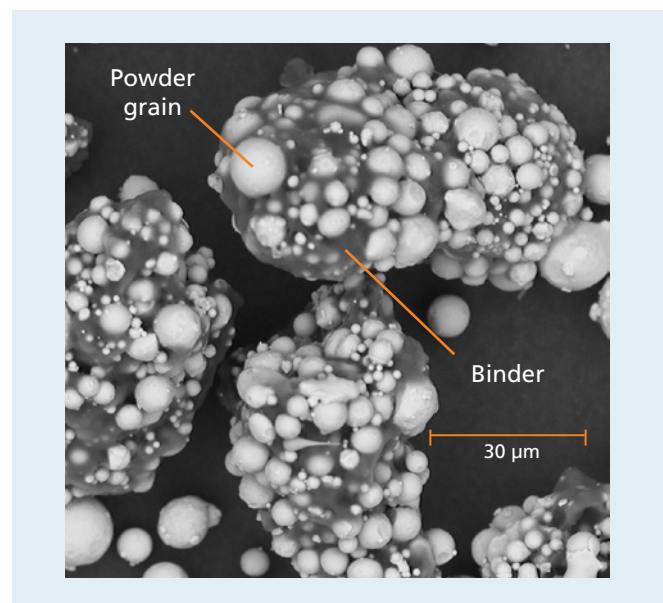


Figure 1: SEM images of 316L powder encapsulated in a polymer matrix [Jul23]

section of the 3D model on the topmost layer, selectively melting the powdered material. This causes the particles to fuse together, creating a solid layer. [Sch15] The build platform is then lowered and a new layer of powder is spread, repeating the process layer-by-layer until the entire object is formed. The unmelted powder acts as a self-supporting bed, eliminating the need for support structures.

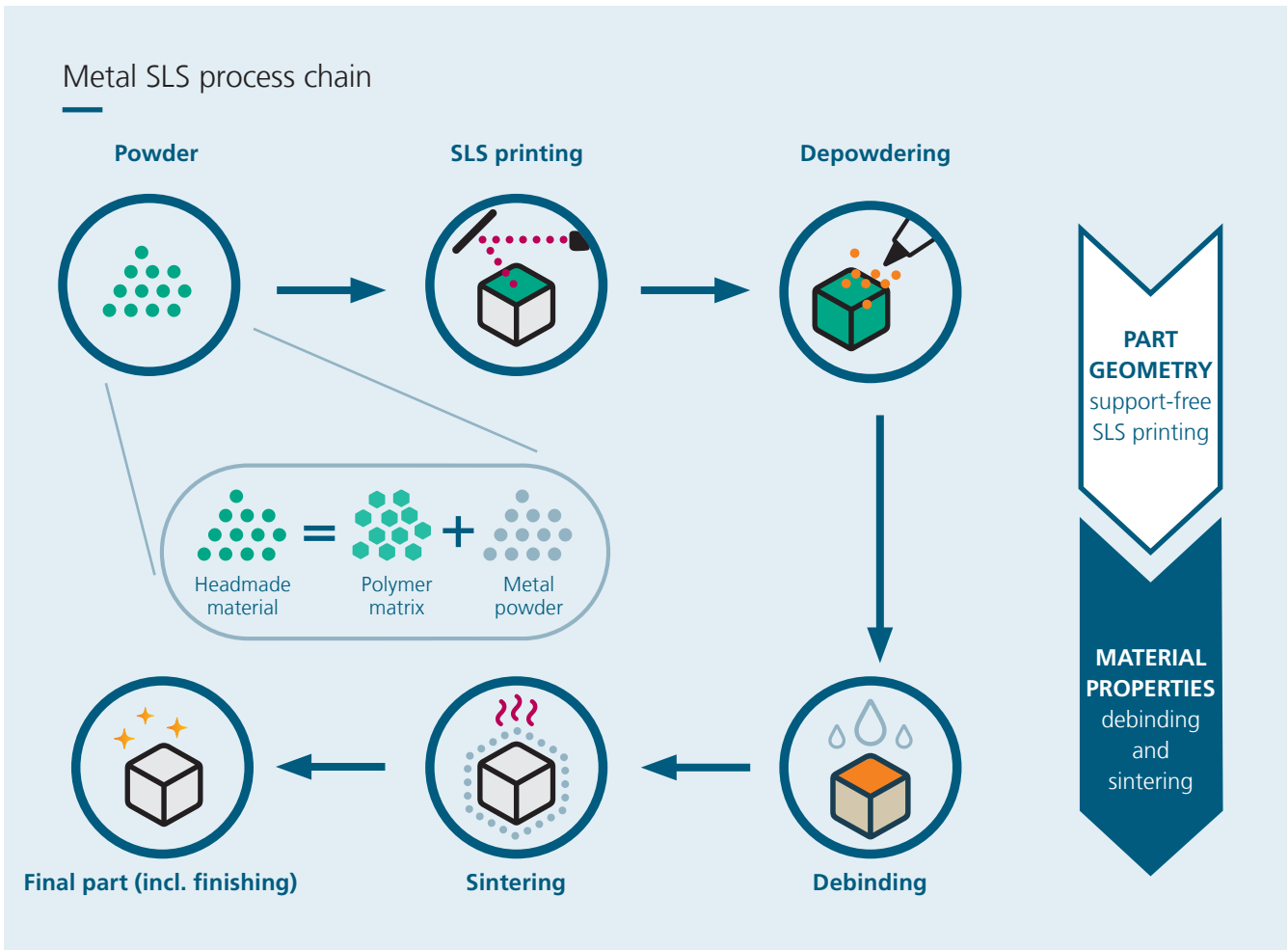


Figure 2: Metal SLS process chain

## Depowdering

After the SLS process, the printed green parts must be freed from the unmelted powder in the build chamber. This procedure begins with a manual removal of adhering powder using a brush. The surplus, unprinted powder is subsequently sifted and can be fully recycled once any powder agglomerations are eliminated. Following this, the parts undergo a thorough cleaning within a parts washer, utilizing a powerful water jet to ensure the complete removal of any residual powder. The meticulous removal of all powder residues is of paramount importance, as these remnants could potentially undergo sintering to the part.

## Debinding

During the subsequent debinding process, the polymeric binder is completely removed from the depowdered green part. The debinding process is typically carried out in two stages: solvent debinding and thermal debinding. For the former, the green part is immersed in a solvent that dissolves the main binder, leaving behind a porous structure. The thermal debinding stage involves controlled heating to evaporate the remaining solvent and back-bone polymer, converting the porous structure into a solid pre-sintered part. Successful debinding is crucial to ensure that no residual binders are present in the final product, as they can cause defects or impurities during sintering.

## Sintering

The brown part resulting from debinding is then sintered by heat treatment below the melting temperature of the material. The resulting sintered parts can achieve a residual porosity of less than 1%. The sintering process at the microscopic level involves closing the pores between the metal particles by moving atoms. For Metal SLS parts, this is accompanied by a shrinkage of typically 14%.

## Finishing

Finishing final parts (or even green parts) in additive manufacturing is a crucial step to enhance their mechanical properties, surface finish and overall performance. The specific finishing options can vary depending on the material used, the additive manufacturing process and the desired final product characteristics. The most important finishing processes for green and sintered parts are:

- Sanding and polishing
- Tumbling
- Vibratory finishing
- Painting, coating or plating
- Electropolishing
- Machining (e.g. CNC)
- Thermal Treatment (e.g. HIP)



**Support structure minimal  
part design drastically reduces  
lead time in LPBF.«**

## 7. Methodology

The selection of the appropriate process for a particular application requires a precise consideration of economic and quality factors. In this study, an assessment of these factors is made for Metal SLS as a still fairly new AM process. Likewise, a comparison is conducted with LPBF as an already established AM process. Both metal AM processes differ in their process chains, which can lead to considerable differences in part quality (e.g. material properties, surface quality), cost per unit, lead time and sustainability (e.g. material efficiency).

Therefore, an economic comparison first focuses on the unit costs, lead time and material efficiency for a given demonstrator from the bicycle industry in a realistic batch size. In the subsequent quality comparison, the dimensional stability, density, mechanical properties and surface quality for Metal SLS are investigated and compared with LPBF as a benchmark. The results are summarized at the end of the study, analogous to Table 1, to provide a comprehensive overview of the potentials and challenges of the two AM processes.

### Methodology

Investigated properties		Metal SLS	LPBF
Economical comparison	 Costs per unit		
	 Lead time		
	 Material efficiency		
Quality comparison	 Dimensional accuracy	<b>TO BE DETERMINED</b>	
	 Density		
	 Tensile strength		
	 Ductility		
	 Vickers hardness		
	 Surface quality		

Table 1: Intended summary of the results obtained

# 8. Economical comparison

In order to evaluate the Metal SLS and LPBF process, the economic indicators of cost per unit, lead time and material efficiency are considered in this study. The determination of economic indicators depends heavily on factors such as the build volume or the number of lasers.

A direct comparison between Metal SLS and LPBF process is generally difficult. Therefore, within the scope of this study, two process chains for Metal SLS and LPBF are pre-defined, which are available at Fraunhofer IAPT and serve as a basis for the economical comparison. For the purpose of comparability, the following assumptions are made for these base processes:

- The same build volume is taken for both AM processes (8,042 cm<sup>3</sup>).
- Single-laser machines are used for both AM processes

In addition to the base processes, productivity boosts are investigated, as can be seen in Figure 3. For this purpose, process-specific impact factors are changed that have a strong impact on the overall process chain. Since Metal SLS is a sinter-based AM process, unlike LPBF, a larger furnace volume is analyzed, which generally allows more AM parts to be sintered at once. With LPBF, on the other hand, the number of lasers is quadrupled, so that the process time for the same number of parts is reduced. The effects on lead times and thus also on costs per unit are the focus of the following sections.

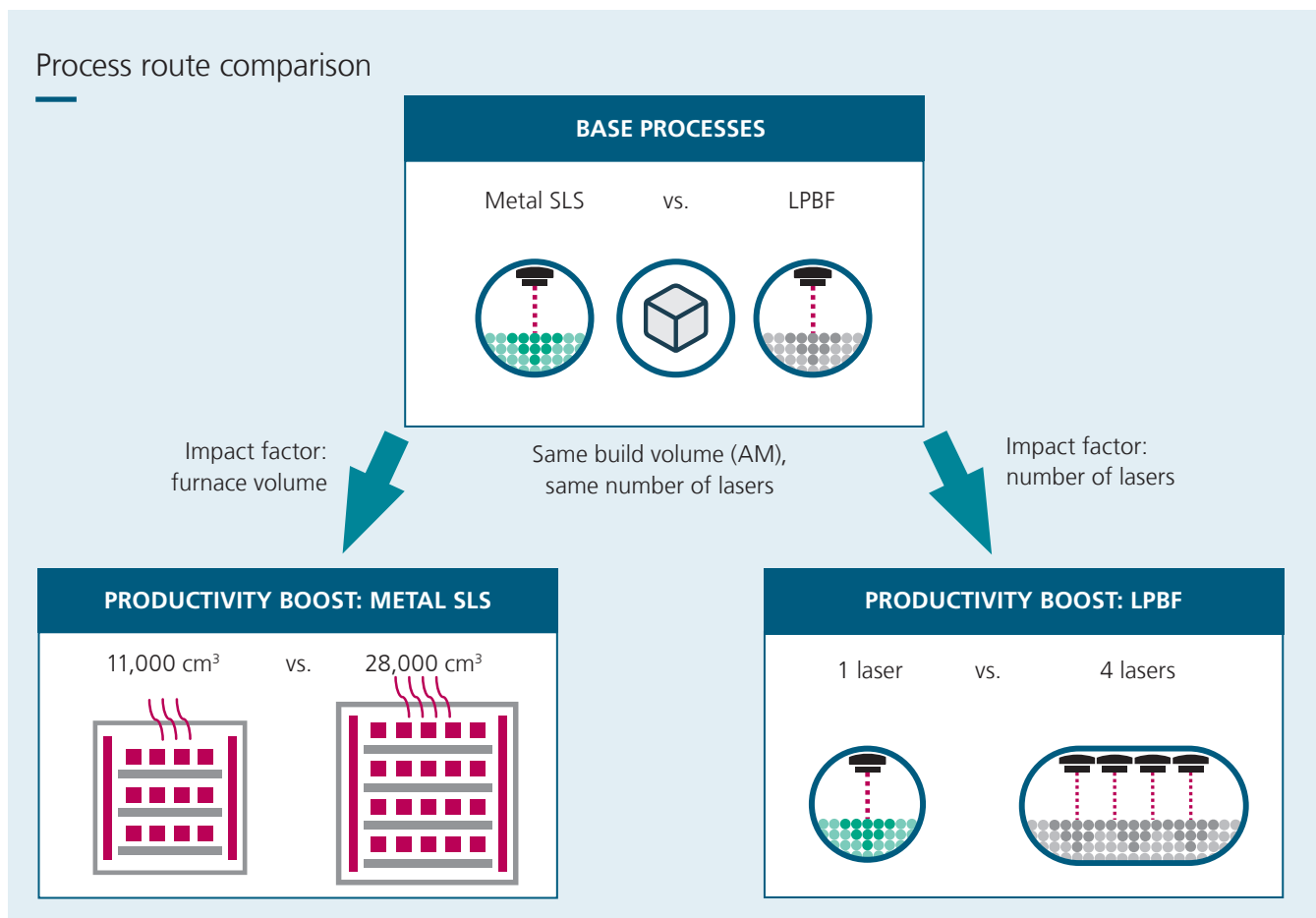


Figure 3: Base processes and process-specific productivity boosts





**Cost-effective production of small and middle batch sizes through Metal SLS.«**

### Demonstrator

The demonstrator for this study serves to compare the different process chains without being specifically optimized for one AM process. The choice of demonstrator is based on a part that can be manufactured by both processes in terms of size and represents a realistic use case. Such a part can be found in high performance cycling where parts are continuously designed to be weight optimized and produced in low to middle volumes. In the »centerlock« brake system, which allows a quick exchange of the brake disk, a connecting element is used between the wheel hub and the brake disk. The structure of such a brake disk mount is visualized in Figure 4. The »brake disk mount« element as a metallic part with lightweight design potential for small and medium batch sizes is ideally suited as a demonstrator for this study. A realistic batch size of  $n = 1,000$  units per year is defined here.

### Investigated material

The demonstrators are made of 316L stainless steel powder, which is commercially available in a process-optimized form for both AM processes. 316L as a material is an austenitic, acid-resistant alloy used in mechanical applications with high requirements and good corrosion properties, such as bicycle

### Brake disk mount demonstrator

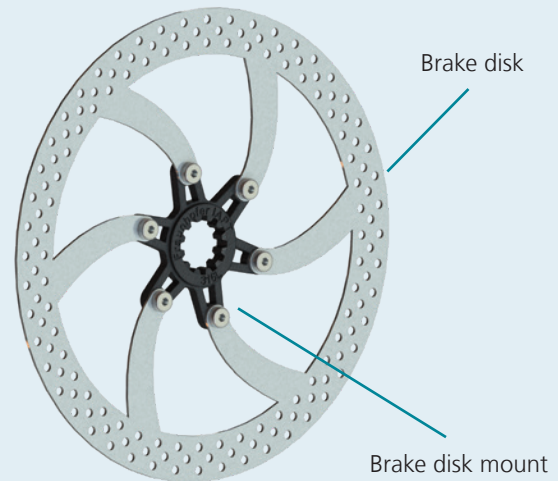


Figure 4: Brake disk mount demonstrator

parts and is therefore particularly well suited for the demonstrator application [Hea22a]. For LPBF, the powder is available atomized in a particle size distribution of 15 - 45  $\mu\text{m}$  and is processed directly [Thy23]. In contrast, the Metal SLS powder is encapsulated in a polymeric binder system in a further step after atomization, resulting in powder particles with a size below 120  $\mu\text{m}$ . The chemical composition of both powders can be found in Table 2.

### Chemical composition of Metal SLS and LPBF 316L powder

Metal SLS 316L powder								
Cr	Ni	Mo	Mn	Si	P	S	C	Fe
16.0-18.0	10.0-14.0	2.00-3.00	$\leq 2.00$	$\leq 1.00$	$\leq 0.04$	$\leq 0.03$	$\leq 0.03$	balanced

LPBF 316L powder								
Cr	Ni	Mo	Mn	Si	P	S	C	N
16.5-18.5	10.0-13.0	2.00-2.50	$\leq 2.00$	$\leq 1.00$	$\leq 0.04$	0.015-0.03	$\leq 0.03$	10.0-13.0

Table 2: Chemical composition (wt.%) of Metal SLS [Hea22] and LPBF [Thy23] 316L powder

## 8.1 Base process: Metal SLS

In AM, the Metal SLS process belongs to the multi-step process chains. Unlike the LPBF process, which produces metal parts in a single step, the SLS process is followed by subsequent debinding and sintering. In order to determine costs per unit and lead time, it is necessary to identify the most influential factors in order to make a fundamental comparison. These influential factors have been compiled in Table 3 and associated with their respective process stages. During the process simulation, the quantitative data of the influencing factors were determined and compared in charts.

### Process chain

The process chain simulation was carried out on the basis of the system equipment available or known at the Fraunhofer IAPT. For the process step of Metal SLS printing, the Sintratec S2 with a build volume of 8 liters was chosen. The debinding of the parts following the printing process is based on the 3D Gence MD12. The subsequent sintering process is simulated by MUT's ISO 240 furnace.

### Influencing factors

Metal SLS process	Debinding	Sintering
<ul style="list-style-type: none"> <li>■ Part volume</li> <li>■ Support-material volume</li> <li>■ Powder costs</li> <li>■ Process time</li> <li>■ Energy consumption</li> <li>■ Gas consumption</li> <li>■ Consumables</li> </ul>	<ul style="list-style-type: none"> <li>■ Energy consumption</li> <li>■ Solvent loss</li> <li>■ Consumables</li> </ul>	<ul style="list-style-type: none"> <li>■ Energy consumption</li> <li>■ Gas consumption</li> <li>■ Consumables</li> </ul>
Pre-/Postprocessing	General	
<ul style="list-style-type: none"> <li>■ Process preparation</li> <li>■ Unpacking</li> </ul>	<ul style="list-style-type: none"> <li>■ Maintenance</li> <li>■ Depreciation</li> </ul>	

Table 3: Influencing factors on the Metal SLS process chain

### Lot-size calculation

Process	Parts per build jobs		Parts per batch (1,000 pcs)	
	Maximum capacity	Quantity of jobs	Maximum capacity	Quantity of jobs
SLS	220	1	1,100	5
Debinding	144	1	1,008	7
Sintering	185	1	1,110	8

Table 4: Metal SLS process route comparison between parts per build job and batch

### Batch size

The process times for producing the parts in the printer are calculated by the build processor in the Sintratec Central software for build preparation. The demonstrators were placed in the plane with maximum space utilization and stacked with a height spacing of 1 mm up to the maximum filling height. This arrangement allowed 220 demonstrators to be produced in a single run. The arrangement in the software is shown in Figure 5.

In order to establish comparability and mitigate the scale effect in the subsequent processes, a batch size of 1,000 demonstrators are examined. Table 4 presents the maximum capacity per process step, which is then multiplied by the requisite factor to attain a batch size of 1,000 demonstrators. It also provides a breakdown of the quantity of each job per process step.

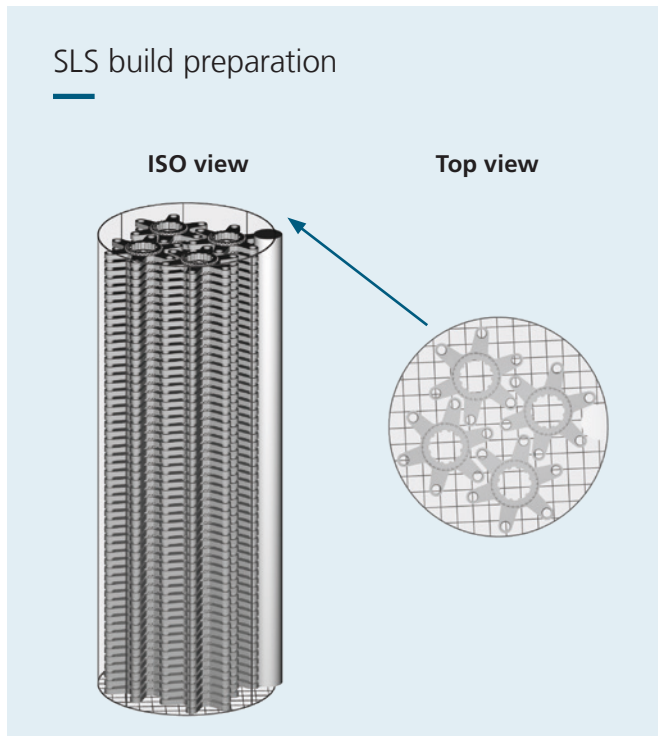


Figure 5: Build part preparation in Sintratec Central



### Costs per unit

Along the process chain, the relevant consumptions were recorded and visualized in Figure 6 with the respective costs of the powders and consumption prices. The bar chart shows the breakdown of the process chain into its individual steps, leading to a unit cost of 10.09 €. Among the most impactful economic factors within this chain are the preprocessing expenses attributed to manual labor as well as equipment depreciation. The depreciation per unit is calculated by considering the machine's annual depreciation rate and the theoretical annual number of build jobs it can handle, without factoring in any potential downtimes. Consequently, any maintenance or repair requirements contribute to an increase in the depreciation expenses. It's worth highlighting that the debinding process step has minimal impact on the part's overall cost due to its low energy and acetone consumption.

### Lead time

The process times for printing, debinding and sintering are evenly distributed across all stages, even though the machines undergo varying numbers of cycles. A batch of 1,000 demonstrators completes the entire process chain in 341 hours, as illustrated in Figure 7. The pre- and postprocessing times have a relatively large share in this process chain, due to the number of cycles per process step that result from the relatively small machine volumes.

Given that the debinding machine goes through the most cycles and has the lowest acquisition costs in the process chain, optimal productivity and economic efficiency can likely be attained by utilizing a debinding machine with a larger capacity or implementing a redundant machine design.

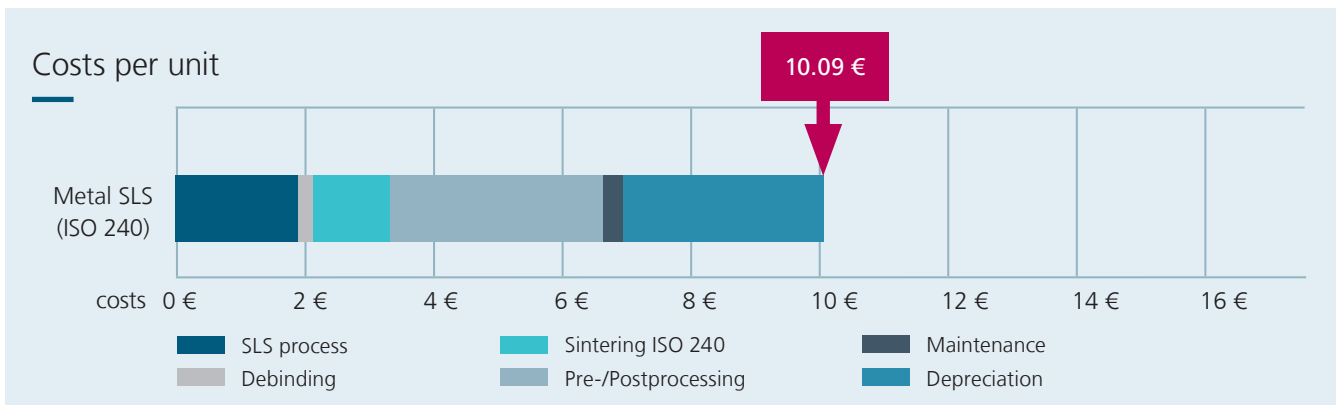


Figure 6: Costs per unit for Metal SLS with ISO 240 furnace

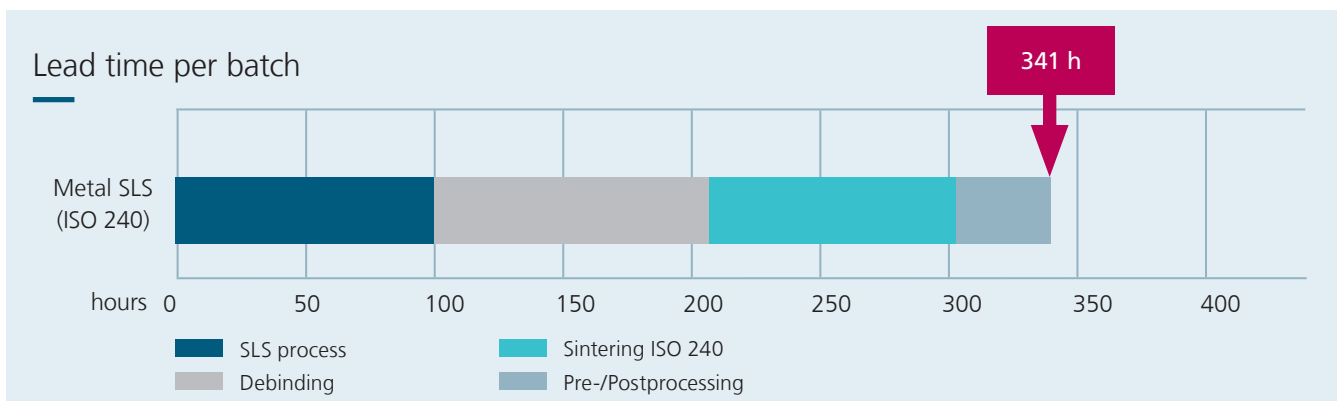


Figure 7: Lead time for Metal SLS with ISO 240 furnace

## 8.2 Base process: LPBF

To compare the single laser Metal SLS system with a single laser LPBF system, an analogous analysis is conducted. Given the differences between the machines and their configurations, the build volume is standardized to match that of the Metal SLS machine. The LPBF single-step process, characterized by the direct production of parts without intermediate stages, significantly influences lead time. Additionally, the design of part geometry plays a crucial role, exerting a substantial impact on postprocessing efforts, such as support removal and consequently affecting both costs and lead times. To deepen this investigation, the various influencing factors from Table 5 are examined using the bike demonstrator.

### Process chain

As a complement to the Sintratec S2 in the Metal SLS process, the LPBF simulation is carried out with an EOS M 290. After printing, the parts are separated from the platform by wire-cut Electrical Discharge Machining (EDM) and manually reworked to remove any adhering support structures.

### Batch size

The process preparation of the demonstrators with the support generation was performed in Materialise Magics. On the build platform, the demonstrators were provided with the spacing of an EDM wire diameter of 0.2 mm in height, which means that most of the support is removed automatically. Only the height difference between the inner ring and the outer arms leaves support structures that have to be removed manually afterwards. The parts were placed in the plane and stacked to the maximum height due to the chosen volume height limit. This arrangement thus allows 550 demonstrators to be produced in one build job, which is visualized in Figure 8. The process time calculation was then simulated in the EOS Print software.

Compared to a large number of cycles per process step in Metal SLS, two cycles are required to produce 1,000 demonstrators in the single laser LPBF machine. Depending on the material, heat treatment or Hot Isostatic Pressing (HIP) may be necessary to achieve the required material properties. For the material 316L, this was not necessary for this part size. This comparison is shown in Table 6.

### Influencing factors

LPBF process	Eroding
<ul style="list-style-type: none"> <li>■ Part volume</li> <li>■ Support-Material Volume</li> <li>■ Powder costs</li> <li>■ Process time</li> <li>■ Energy consumption</li> <li>■ Gas consumption</li> <li>■ Consumables</li> </ul>	<ul style="list-style-type: none"> <li>■ Energy consumption</li> <li>■ Wire costs</li> </ul>
Pre-/Postprocessing	General
<ul style="list-style-type: none"> <li>■ Process preparation</li> <li>■ Unpacking</li> <li>■ Support removal</li> </ul>	<ul style="list-style-type: none"> <li>■ Maintenance</li> <li>■ Depreciation</li> </ul>

Table 5: Influencing factors on the LPBF process chain

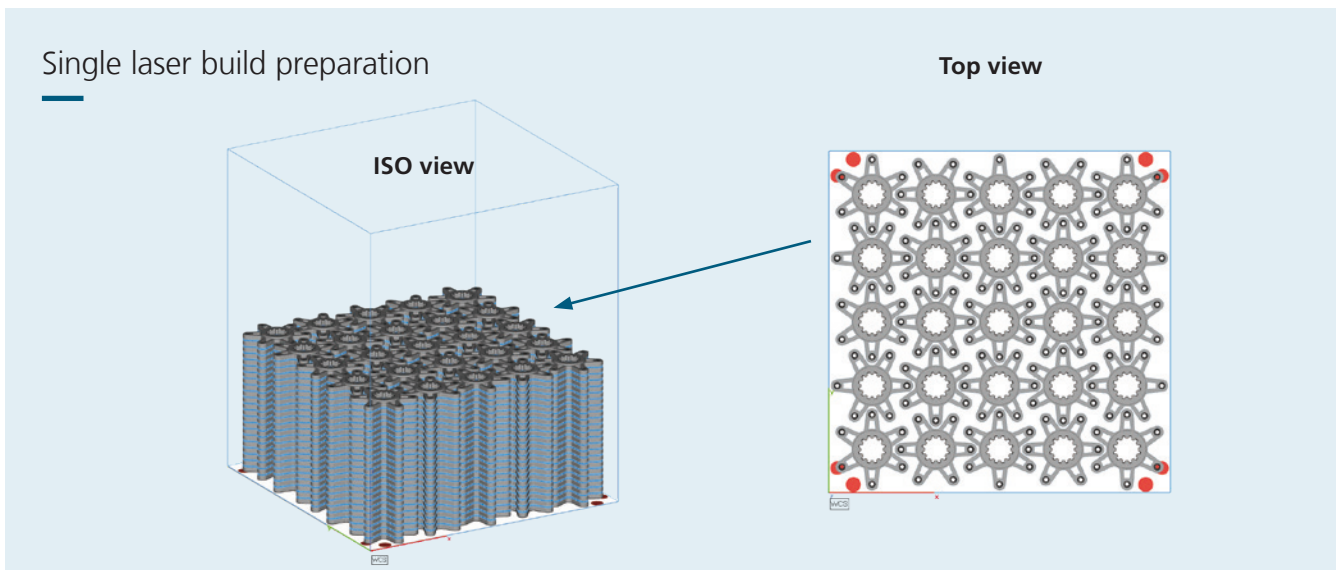


Figure 8: Build part preparation in Materialise Magics

### Lot-size calculation

Single laser LPBF process chain		
Process	Maximum capacity	Quantity of jobs
LPBF	1,100	2
Eroding	1,100	2

Table 6: Lot-size calculation for 1,000 manufactured demonstrators in single laser LPBF

### Costs per unit

The graphical representation in Figure 9 illustrates the breakdown of the costs within the single laser LPBF process chain. The process costs for LPBF manufacturing and eroding are comparable to Metal SLS manufacturing with subsequent debinding and sintering. Since the production of parts in the LPBF involves the use of support structures, the removal of these requires a high amount of time and therefore high labor costs due to the manual rework.

Additionally, the high initial acquisition costs of the LPBF system and the wire EDM machine contribute to a substantial part of depreciation costs per part, which are comparatively lower in the Metal SLS process chain due to its lower initial investment requirements. This is particularly true for the Sintratec S2, whereas other industrial machines with a higher purchase price would also increase the depreciation amount. Including all process costs, the unit price for the LPBF manufactured demonstrator is three times more expensive at 33.29 €.

### Lead time

Along with the comparison of process costs, the lead time is analyzed in Figure 10. Compared to the results from the Metal SLS base process the production of a similar quantity single laser LPBF manufactured demonstrators leads to a 54 % increase in lead time. This is mainly due to the three and a half times longer manufacturing time in LPBF as well as the relatively high postprocessing effort. The printing process time is mainly influenced by the layer height, for which standard values were used for both AM processes. The production of the LPBF manufactured demonstrators was simulated with a 60 µm layer height, whereas the layer height of the Metal SLS manufactured demonstrators was 100 µm. The layer height in the Metal SLS process is largely determined by the particle

size of the powder. With a lower layer height, the number of exposures as well as coatings per layer increases, which has a significant impact on the manufacturing time. Higher layer thicknesses in LPBF are possible, but are accompanied by a decrease in surface quality.

The distance between the demonstrators was equal to the diameter of the EDM wire, so that the surfaces were removed smoothly and only minor supports remained on the surface. Eroding the 1,000 demonstrators resulted in a process time of 200 hours, requiring an additional 167 hours of manual post-processing time. Overall, the production of all demonstrators requires 341 h in the Metal SLS process and 742 h in the LPBF process. However, the postprocessing effort can be further reduced by a process-adapted part design in LPBF.

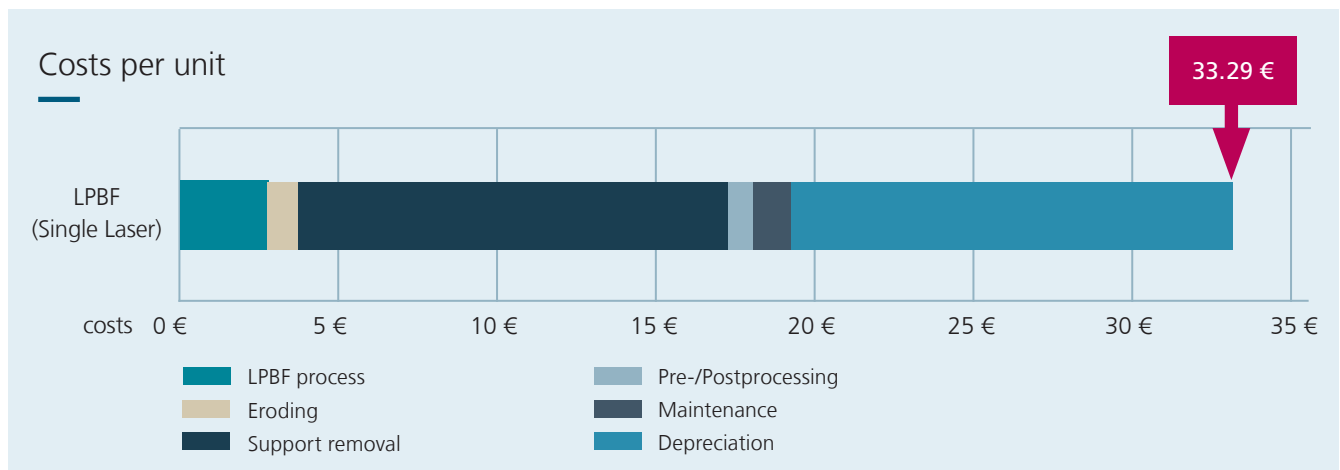


Figure 9: Costs per unit for single laser LPBF

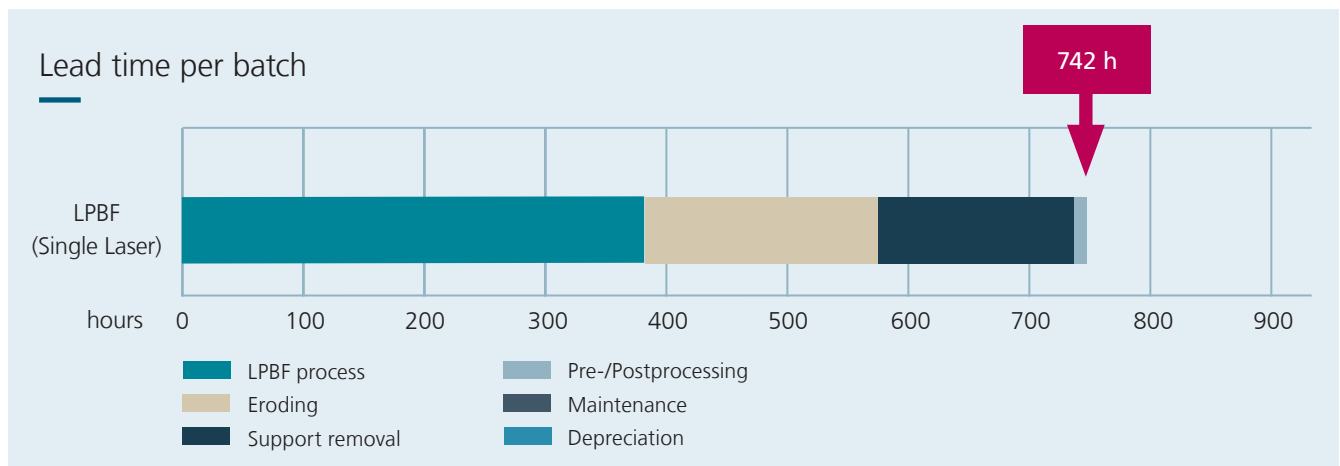


Figure 10: Lead time for single laser LPBF



## 8.3 Productivity boost: Metal SLS

Within the Metal SLS process chain, the furnace volume can be expanded relatively inexpensively. Doubling the furnace volume is accompanied by an increase in acquisition costs of approximately 15 %. This increase allows for the operation of the furnace with a higher batch size, leading to reduced process costs and lead times. Additionally, under full furnace utilization, it results in a reduction in depreciation costs per part. The impact of doubling the furnace volume on both unit costs and lead time is illustrated below.

### Costs per unit

Achieving the maximum utilization within one sintering run in ISO 320 results in costs per unit of 8.93 €, which is a 12 % reduction in cost per unit compared to ISO 240 furnace. The slightly increased initial cost of the furnace is spread over the amount of parts, which in turn are quickly amortized by the lower operating costs. Preprocessing costs are also slightly reduced due to the lower number of sintering cycles for which the furnace has to be prepared. The detailed process step representation is visualized in Figure 11.

### Lot-size calculation

Process	Metal SLS with ISO 320	
	Maximum capacity	Quantity of jobs
SLS	1,100	5
Debinding	1,008	7
Sintering	1,449	3

Table 7: Lot-size calculation per sinter run in Metal SLS process route

### Costs per unit

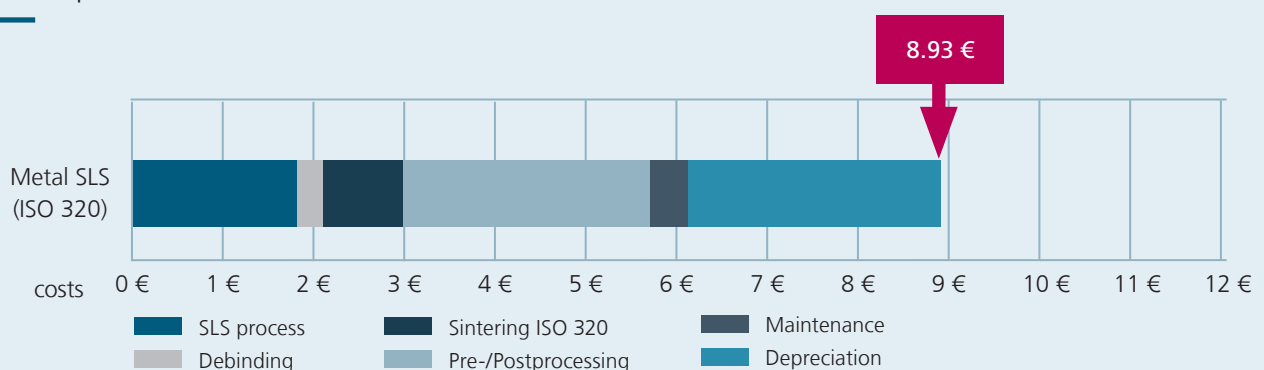


Figure 11: Costs per unit for Metal SLS with ISO 320 furnace

### Lead time

The lead time for the same number of demonstrators is identical for the Metal SLS process as well as for the debinding process step. Only the furnace times and the associated preprocessing times are reduced when using a 2.5 times larger

furnace volume. Due to the larger furnace volume, the same number of demonstrators can be sintered with fewer cycles, reducing the lead time by 16 % to 287 hours. The comparison of the lead times of the two process routes are shown in Figure 12.

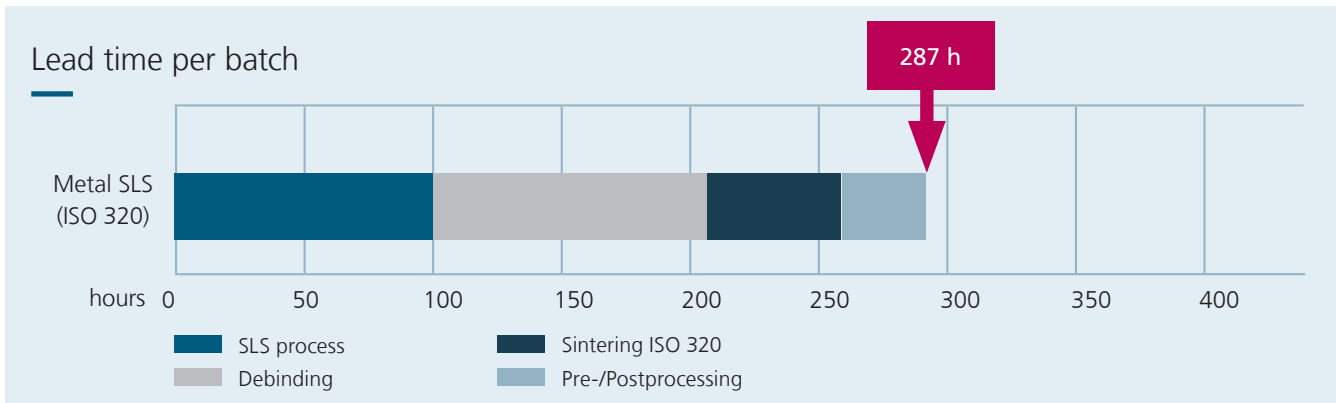


Figure 12: Lead time for Metal SLS with ISO 320 furnace



## 8.4 Productivity boost: LPBF

The incorporation of multi-laser systems translates into enhanced productivity throughout the manufacturing process. When the build volume scales proportionally with the increased number of lasers, it also results in reduced recoating times, given that parts can be optimally distributed within the plane. In this study, the influence of a quad laser system with a build plane 2.4 times larger and a build volume 2.5 times larger was investigated. As with the single laser LPBF process route, all influencing factors from Table 5 were examined.

### Process chain

For the productivity boost, the EOS M 290 was replaced with an SLM500 quad laser system. The EDM and support removal following the manufacturing process remain unchanged.

### Batch size

The process preparation for the demonstrators was also conducted using Materialise Magics. Similar to the single laser LPBF machine and Metal SLS machine, the quantity of demonstrators varies due to their arrangement on the build platform. The build height of an identical build volume is reduced compared to the single laser LPBF system, because of the larger base plate.

A more efficient stacking of the demonstrators in terms of height resulted in fewer parts being optimally placed within the given area, resulting in a 28 % reduction in the number of parts produced. The process time was computed using SLM Solution's build processor within Materialise Magics. The arrangement of the demonstrators is depicted in Figure 13. Compared to the single laser LPBF machine, with 550 parts per cycle, a total of three cycles have to be made in the quad laser LPBF machine to produce a quantity of 1,000 demonstrators.

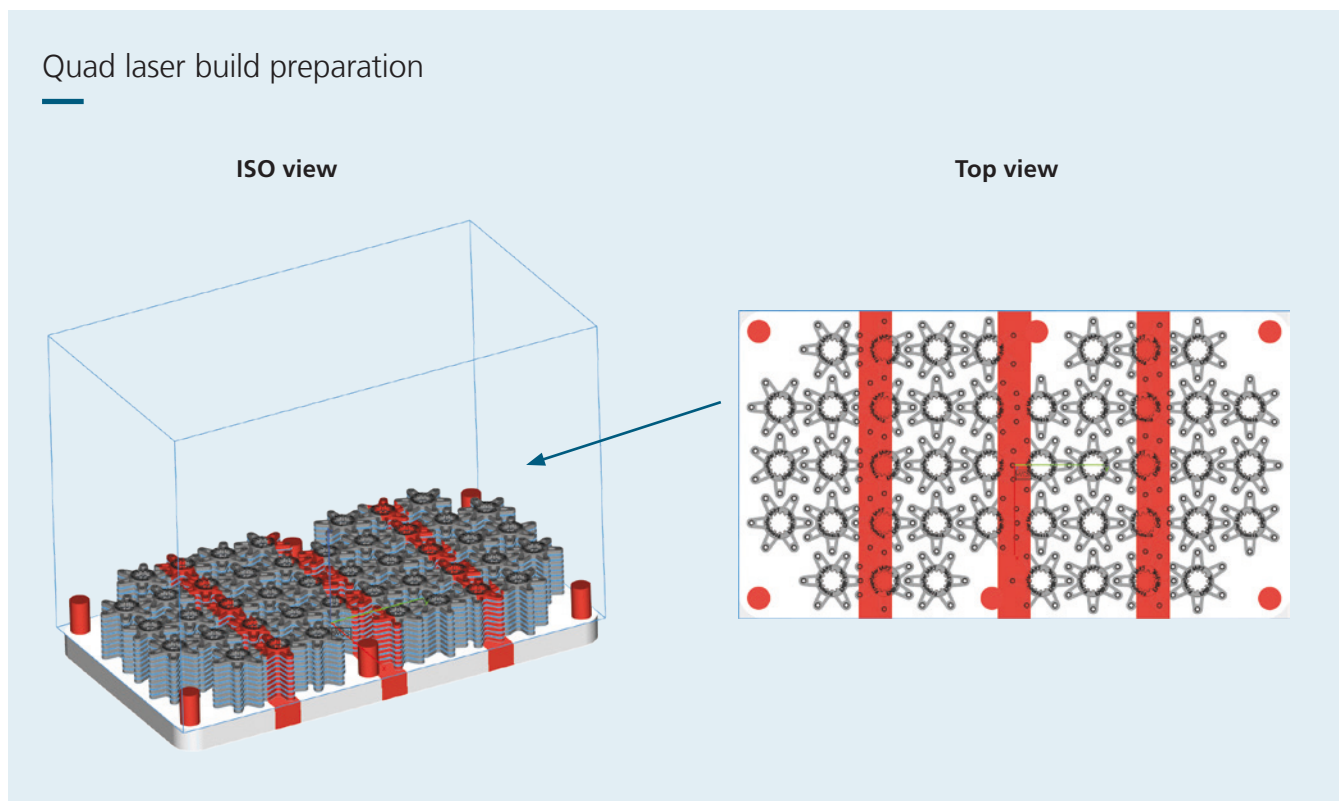


Figure 13: Build part preparation in Materialise Magics

### Lot-size calculation

Quad laser LPBF process chain		
Process	Maximum capacity	Quantity of jobs
LPBF	1,188	3
Eroding	1,188	3

Table 8: Lot size calculation for 1,000 manufactured demonstrators in quad laser LPBF

### Costs per unit

Compared to the Metal SLS process chain, the high depreciation due to the high equipment costs and the high costs for the large amount of postprocessing effort become apparent for the LPBF process chain. The unit cost of the demonstrators in the Metal SLS process chain is 75 % lower compared to the quad laser LPBF system, mainly due to these two factors. The cost to produce the 1,000 demonstrators increased to 40.41 € compared to the single laser machine. For parts manufactured by LPBF, the aim is thus to keep the post-processing effort as low as possible, e.g. through a parts design that requires as few supports as possible. The created data for the costs per unit are shown in Figure 14.

### Lead time

Within the LPBF process, the lead time of the demonstrators are primarily influenced by the manufacturing time within the machine, which is visualized in Figure 15. Despite achieving higher productivity, the quad laser LPBF machine experiences only a 19 % reduction in process time with 675 h compared to the single laser LPBF machine, owing to suboptimal utilization. Here, the parts are also serperately separated from each other via wire EDM, leaving a part of the support structure on the outer arms. This must be removed manually, which means that 167 hours must be invested in manual support removal.

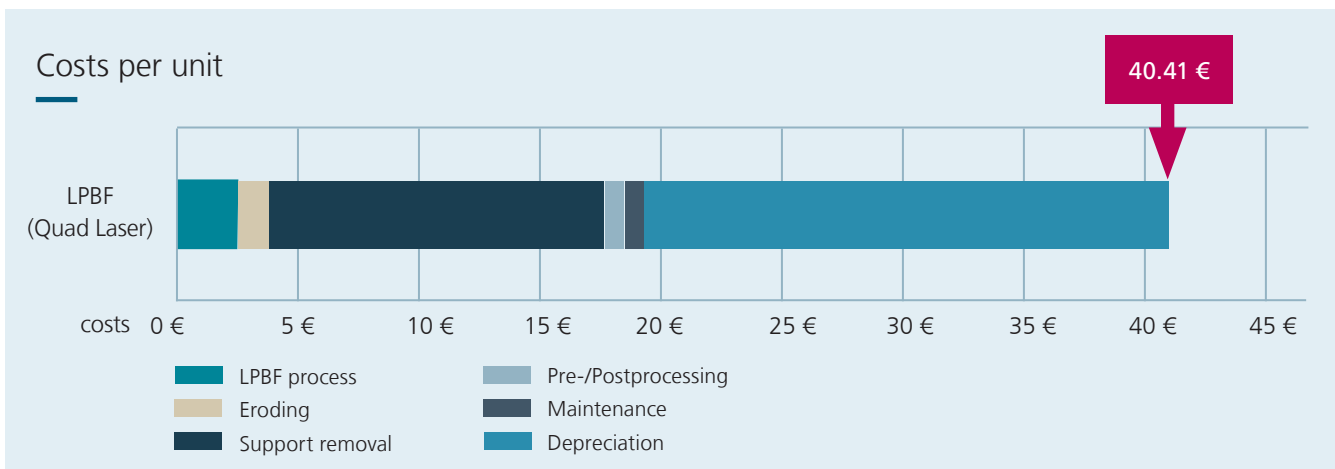


Figure 14: Costs per unit for quad laser LPBF

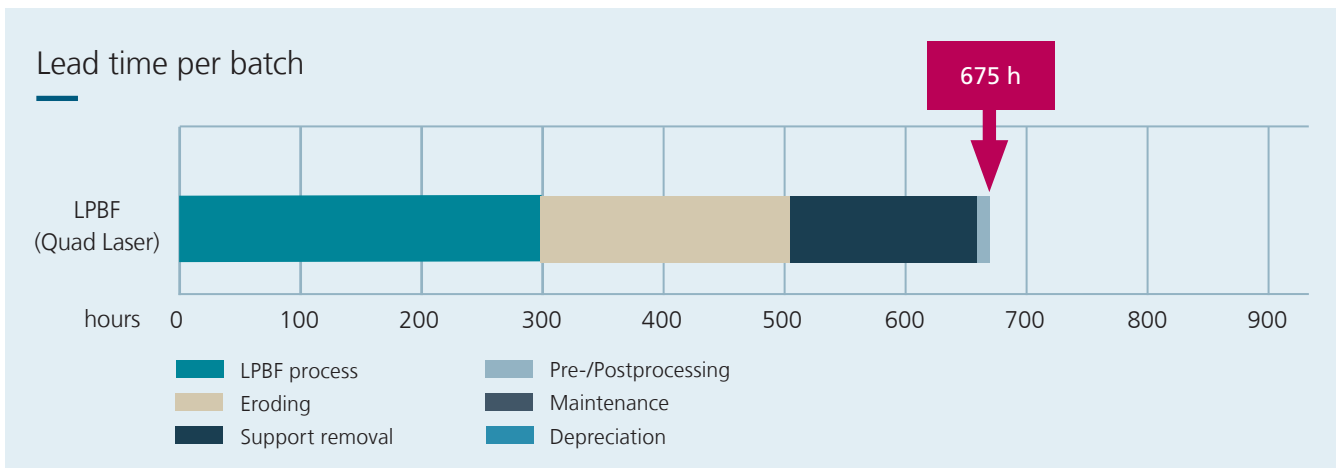


Figure 15: Lead time for quad laser LPBF



## 8.5 Economic evaluation

A comprehensive analysis of both Metal SLS and LPBF process chains highlights the considerable potential of the sinter-based approach compared to LPBF. This holistic view, as depicted in Figure 16 and Figure 17, underscores how the sintering process route not only leads to a more cost-effective production of parts but also shorter lead times.

The printing costs of Metal SLS demonstrators are slightly more economical compared to their single laser LPBF counterparts, falling within the same order of magnitude. This cost advantage in Metal SLS, despite its powder being approximately four times more expensive per kilogram, is offset by the extended running time and the resulting higher consumption of energy and inert gas in the LPBF process. Additionally, the significant manual rework and depreciation costs in LPBF are readily apparent.

The printing time of the LPBF process is about three times longer than in the SLS process. Thus, the production of a

batch in the LPBF process takes about as long as the entire Metal SLS process chain. Efficiency is primarily governed by the process-oriented design of parts, with the primary goal being the minimization of non-productive process time. Process-adapted part design, especially for LPBF parts, can significantly reduce ancillary process costs and lead times, in this case up to 25%. Moreover, the comparison of furnace sizes highlights the lower sintering costs and lead times, clearly visible in the bar charts, attributed to the more efficient operation of the sintering furnace. Additionally, pre- and postprocessing expenses as well as maintenance and depreciation costs experience a slight reduction due to the improved utilization of equipment.

When selecting a production technology, it is crucial to consider various types of equipment within a process chain, particularly under full capacity utilization, to achieve the lowest unit costs and lead times.

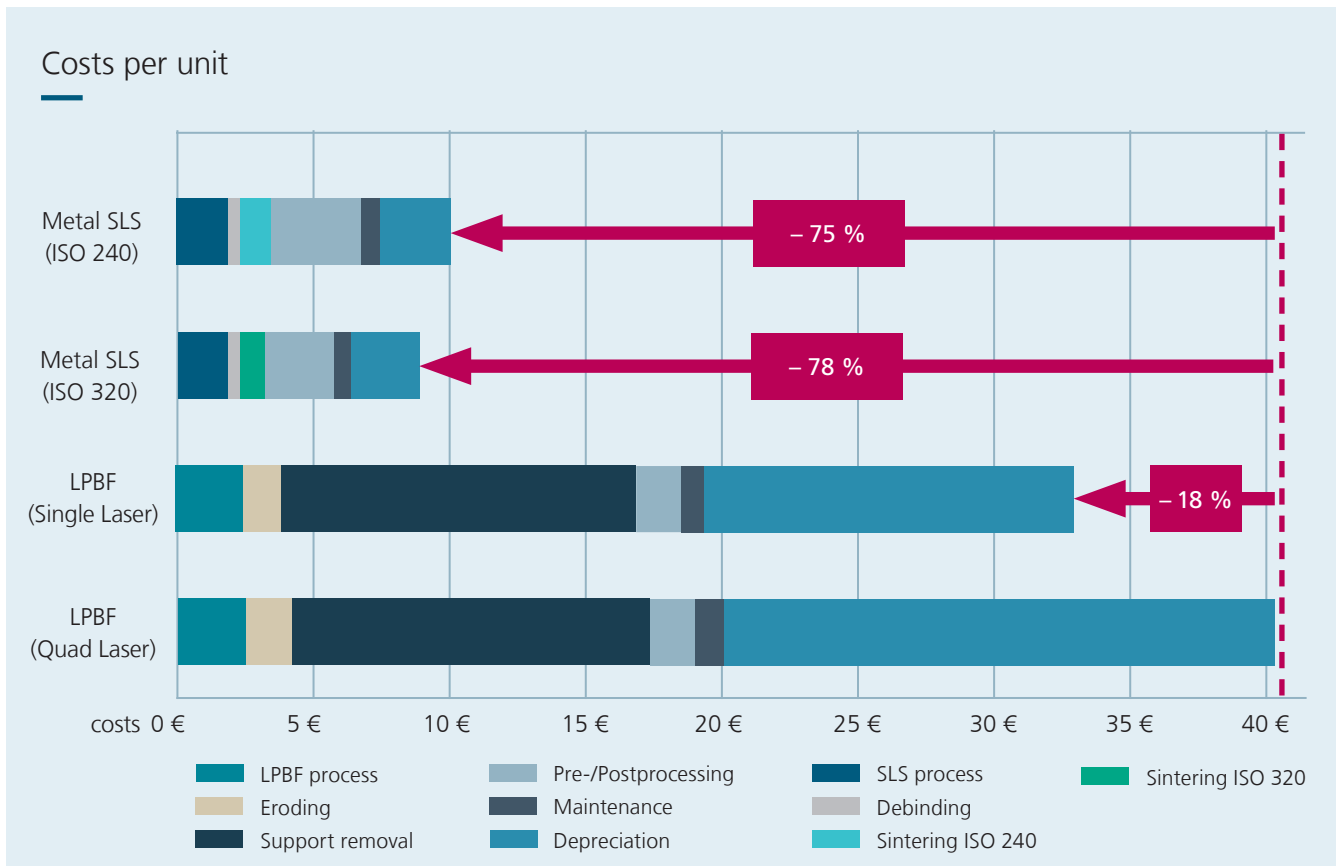


Figure 16: Holistic comparison of cost per unit between Metal SLS and LPBF process routes

## 8.6 Material efficiency

The evaluation of material efficiency results from the total amount of powder material used in the build process, as well as the powder that is lost in the pre- and postprocessing stages within the SLS and LPBF processes. During in both AM processes, the excess powder remaining around the manufactured part is recovered. This is done by vacuuming or manual skimming, followed by sieving of the collected material to remove the coarse grain content. However, residue-free recovery of the non-printed powder is challenging, as the powder accumulates in gaps around the build platform and within the support structures. These non-printed powder residues are removed by a separate vacuum unit, which are subsequently disposed of. The observed loss of the powder material used after each construction phase amounts to 2 %, according to experience. The support structures used in the LPBF during the manufacturing process and in the Metal SLS as sintering supports also contribute to lower material efficiency, as they are removed at the end of the manufacturing process and disposed of.

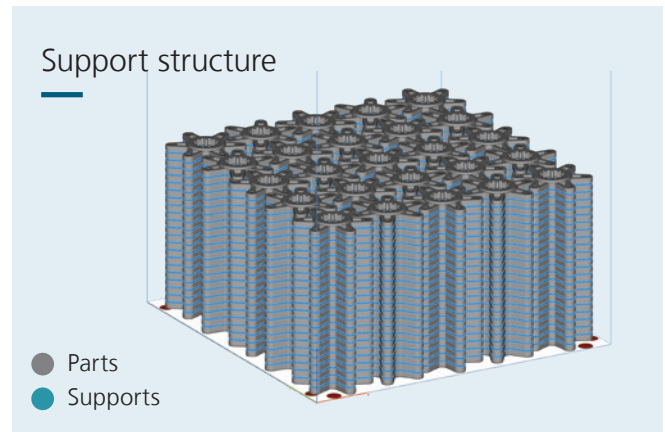


Figure 18: Material efficiency in build job

Optimizing process parameters and a low-support structure build part design thus contribute to an increase in material efficiency. While in this study the Metal SLS demonstrators were manufactured free of support structures, an additional 268 cm<sup>3</sup> was invested for support structures in the single laser and 162 cm<sup>3</sup> in the quad laser LPBF process. Accordingly, the support structures account for 9.2 % for single and 7.9 % in quad laser LPBF of the total print volume (averaged over both systems: 8.6 %). This is associated with an additional cost of 0.43 €/cm<sup>3</sup> and 4.2 min/cm<sup>3</sup> and 0.46 €/cm<sup>3</sup> and 3.4 min/cm<sup>3</sup> respectively. The visualization of the support structure is shown in Figure 18.

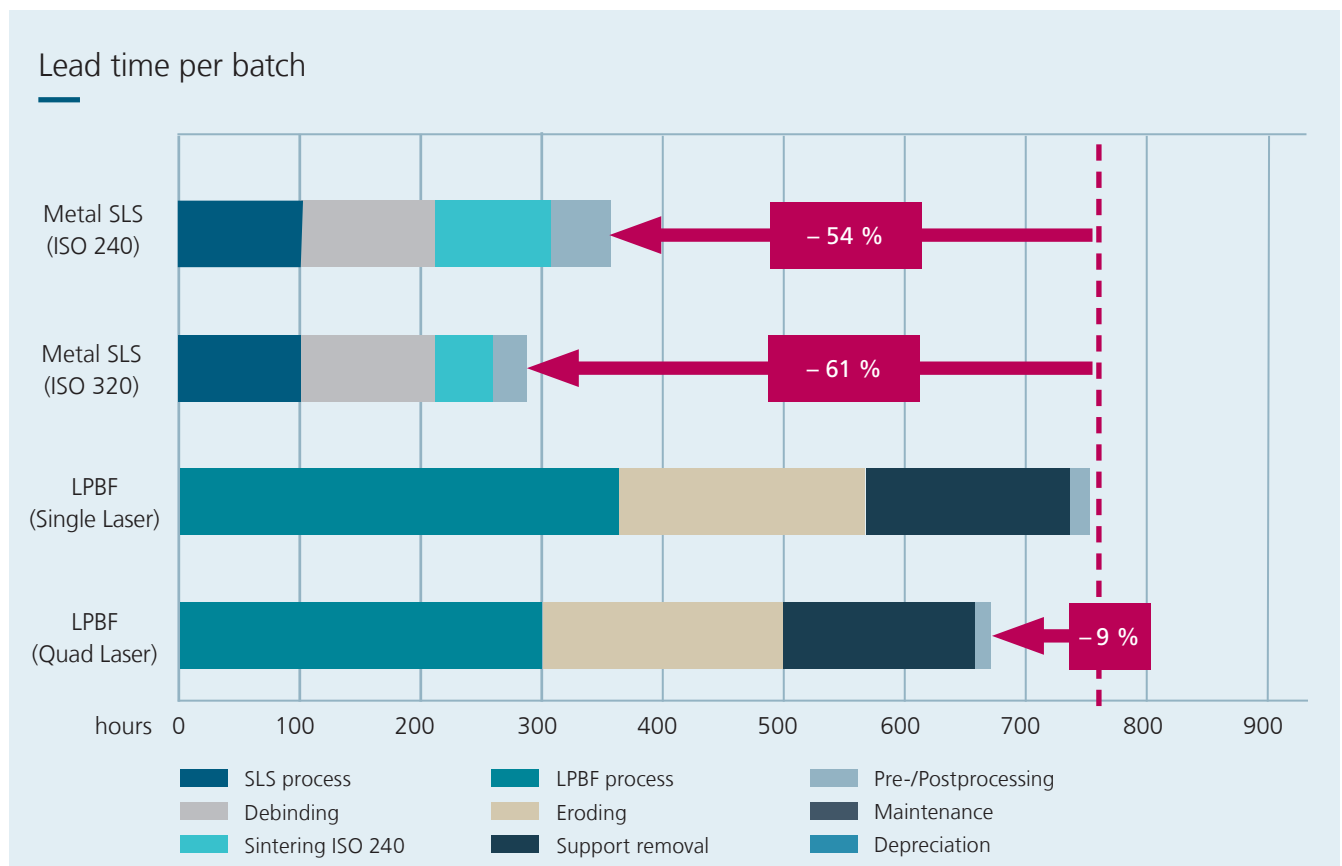


Figure 17: Holistic comparison of lead times between Metal SLS and LPBF process routes



**Metal SLS can be integrated  
as a complementary process in  
the MIM process chain.«**



## 9. Quality comparison

In the experimental part, density cubes, tensile and surface specimens and the demonstrator are produced using Metal SLS and LPBF. With the help of these specimens, the dimensional accuracy, density and microstructure are first investigated. Subsequently, the tensile properties and hardness are evaluated as representative of the mechanical properties. A summary of the experiments including a matching of the specimens can be found in Table 9.

For both Metal SLS and LPBF, due to conflicts of interest, no information can be provided on the detailed process parameters for the preparation of the specimens. However, both parameter sets are based on industry standards. For

Metal SLS, the following equipment technology was used to prepare the Metal SLS specimens:

- SLS printing: EOS Formiga P110
- Debinding: Lömi EDA 30
- Sintering: Carbolite Gero HTK 25

Due to system availability, the SLS printer from the economic comparison (Sintratec S2) had to be replaced by an industrial system (EOS Formiga P110). The LPBF specimens were produced on an industrial EOS system (EOS M 290) and tested as-built without post heat treatment.

### Test methods

	Dim. accuracy	Density	Tensile properties	Hardness	Surface quality
Cubes	X	X		X	
Tensile specimens			X		
Surface specimens					X

Table 9: Matching of the samples to the investigated properties

## 9.1 Dimensional accuracy

In the LPBF process, the metallic powder particles are welded together by laser energy to form a dense structure. In sinter-based AM processes, however, the component is initially present as a fragile green part, in which the metallic powder particles are held together by a binder system. The multi-component binder system is then removed without residue during the debinding and sintering process. Finally, the remaining metal powder is densified by diffusion processes, which leads to significant shrinkage of the metal part. To counteract this shrinkage during the sintering process, the green part is scaled accordingly in the X, Y and Z-directions.

Influencing factors such as the metallic alloy, binder system, particle size or particle size distribution determine, among other factors, the sintering and shrinkage behavior. In addition to the powder binder content, the shrinkage behavior is also determined by the part geometry. Massive or high parts show a different shrinkage behavior to small and unidimensional parts, which may require additional scaling in Z-direction. In

the Metal SLS process, however, the shrinkage of about 14 % can be considered uniform in all directions as in stainless steels such as 316L or titanium alloys such as Ti6Al4V due to the high green part density. [Hea22b]

Shrinkage behavior thus has a significant influence on dimensional accuracy. To investigate this, 10 cubes were manufactured using the Metal SLS process chain from chapter 8. To compensate sinter shrinkage, the green parts were upscaled 14 % in all directions. A 3D profilometer (Keyence VR-6000) was used for the measurement, as exemplified in Figure 19 and Figure 20. The measurement results obtained were then compared with the LPBF benchmark. For this purpose, ten cubes were also produced and measured analogously to the Metal SLS specimens. A summary of the results can be found in Table 10.

The measurement results show that the Metal SLS specimens deviate on average more than 1 % from the target dimensions. Only in the Z-direction did the uniform scaling lead to the

### Cube measurements

Target dimensions		Metal SLS		LPBF	
Axis	Measurements [mm]	Measurements [mm]	Deviations [%]	Measurements [mm]	Deviations [%]
X	10	9.821	- 1.79	9.910	- 0.90
Y	10	9.882	- 1.18	9.906	- 0.54
Z	10	10.017	+ 0.17	9.949	- 0.51

Table 10: Test results for dimensional accuracy

correct dimension with an average deviation of only 0.17 %. The LPBF specimens show on average a marginally better dimensional accuracy with deviations of less than 1 %, which is lowest in the build direction (Z). The reason for this is most likely the layer coating, for which a defined layer is always applied, so that minimal deviations in the Z-direction are leveled out again with each layer.

However, the maximum difference between the dimensional deviations in the Z- and X/Y-direction are observed for Metal SLS. In general, Metal SLS is – in contrast to LPBF – a multistage AM process, so that more process steps have an influence on dimensional accuracy. In addition to the accuracy of AM production, the positioning of the specimens in the sintering furnace, for example, can have a decisive influence. To ensure high dimensional accuracy for sinter-based AM processes such as Metal SLS, the manufacturing conditions (e.g. furnace positioning) must be kept as constant as possible. The green part scaling must then be marginally adjusted accordingly.

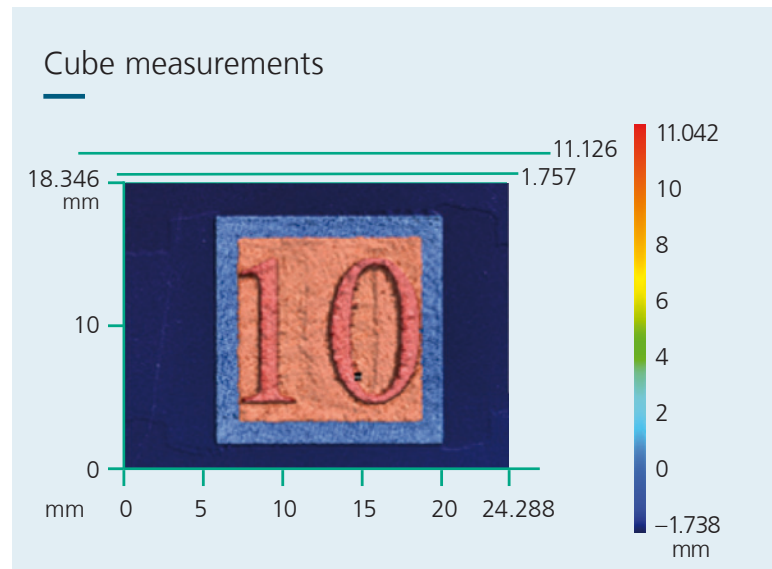


Figure 19: Exemplary measurement of the L-BPF cube 10

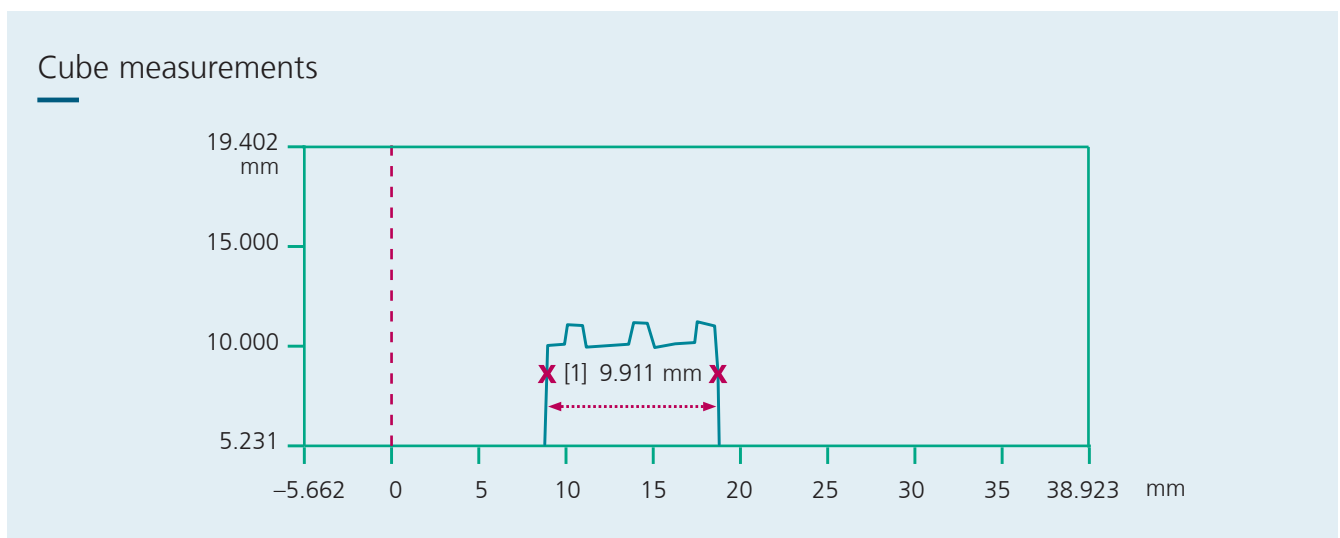


Figure 20: Exemplary measurement of the L-BPF density cube 10

## 9.2 Density

Conducting the density measurements involved a series of procedural steps. Initial warm embedding of all specimens in ClaroFast was performed utilizing a CitroPress-5 from Struers. Sequentially, specimens underwent grinding using SiC grinding foils up to 4000 grit, followed by polishing with the oxide polishing suspension OP-U to achieve a scratch-free finish. Microscopic imaging was carried out using the VHX-5000 digital microscope by Keyence.

Bright light (coaxial lightning) and a 50x magnification were employed for capturing individual images. These discrete images, encompassing sections of the cube surface, were subsequently amalgamated using panorama mode, resulting in a high-resolution composite image.

To assess the density, a software tool developed at Fraunhofer IPT was used, which uses threshold values to distinguish between dark pores and the light polished surface and automatically determines the relative density in the square region of interest (see Figure 21). It is noteworthy that the contour region of all specimens was excluded from this study due to non-optimized contour parameters in the LPBF parameter set

concerning surface porosity. Furthermore, the LPBF specimen geometry was adjusted due to production. The region of interest, however, is comparable and the measurement results are valid.

As already exemplified in Figure 21, the Metal SLS sample exhibits a higher porosity. This impression is also confirmed by the measurement results in Table 11, which shows the density of each individual cube as well as the average value. Accordingly, an average density of 99.25 % can be achieved with Metal SLS and 99.97 % with LPBF.

Since Metal SLS is a sinter-based AM process, a lower density was to be expected. In general, higher densities of up to 99.9 % can be achieved once sintering takes place in the liquid phase. However, the material investigated in this study is usually sintered in the solid phase, which results in a higher porosity. In LPBF, on the other hand, the metal particles are fused together, which, with correctly set process parameters, leads to densities of greater than 99.5 % (see Table 11), which were also measured in this study.

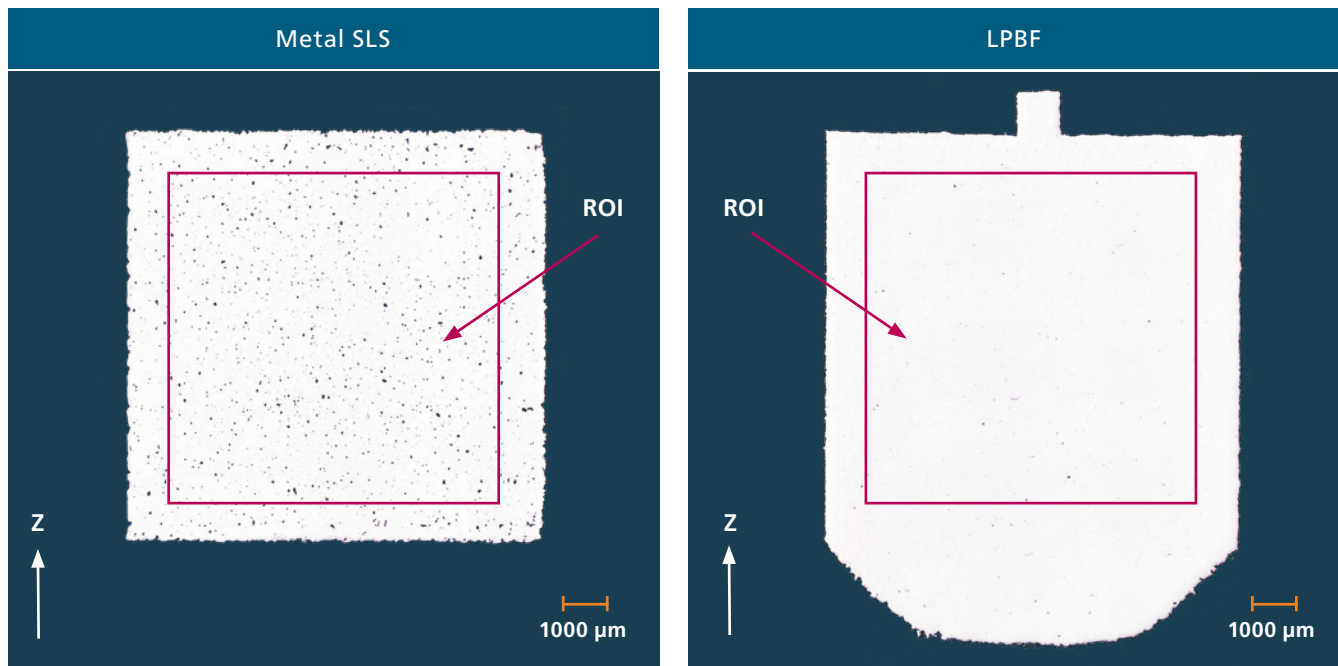


Figure 21: Micrograph analysis of density cube 5 (left: Metal SLS, right: LPBF)

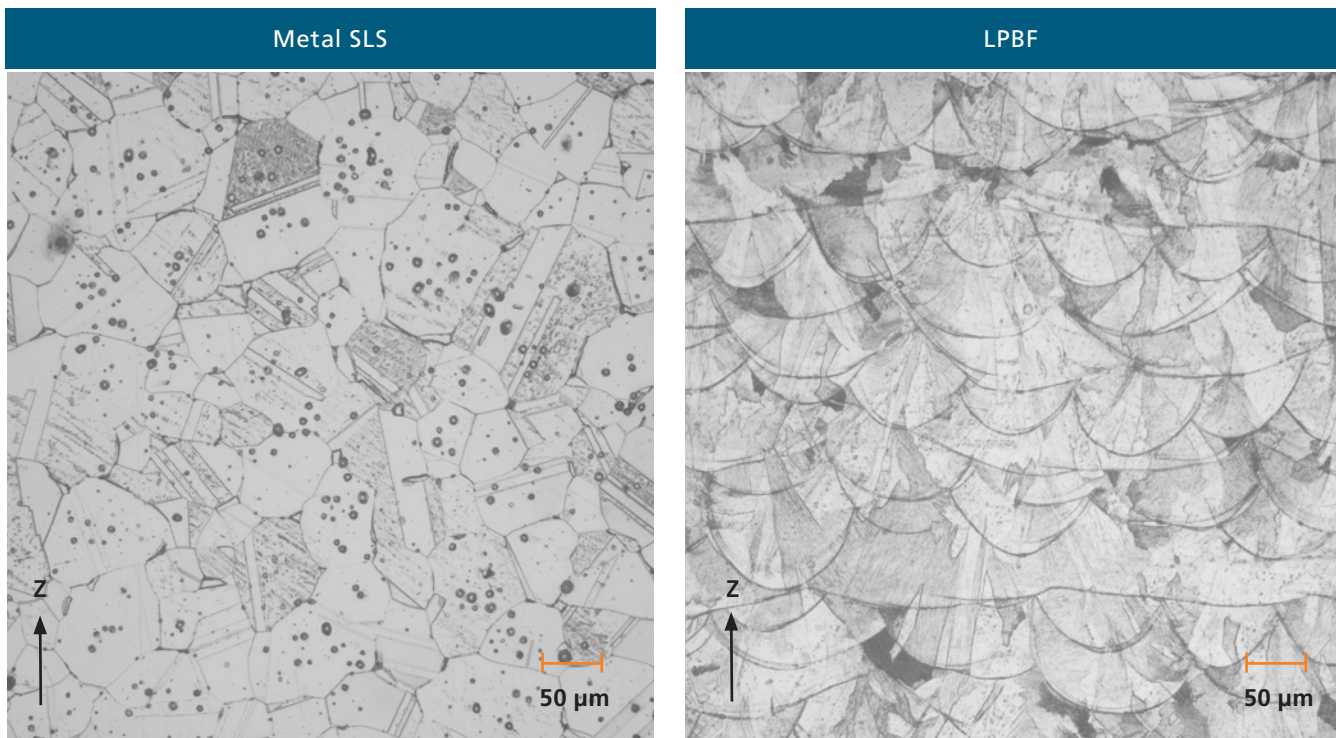


Figure 22: Microstructure of an exemplary Metal SLS (left) and LPBF sample (right)

Following the density measurement, the polished surfaces of the grinded specimens were additionally etched in a V2A acid bath. Then the microstructure was evaluated with a Keyence VHX-5000 digital microscope. The microscope images again confirm the higher porosity of the Metal SLS specimens, which additionally show fine pores due to the sintering process (see Figure 22, left).

### Microstructure

Furthermore, it can be stated that the microstructure is different despite the same material. The reason for this is the temperature history, which is characterized by diffusion-driven densification mechanisms during the sintering process in the case of Metal SLS and by a micro-welding process in the case of LPBF. The weld lines are clearly visible in Figure 22 on the right. Less clearly visible is the grain structure, which, in contrast to Metal SLS, appears to be anisotropic and elongated along the Z-direction. However, based on the temperature history, it can be assumed that the microstructure in Metal SLS is more coarsely grained due to longer holding times at elevated temperatures.

### Density measurements

Cube No.	Relative density [%]	
	Metal SLS	LPBF
1	99.06	99.96
2	99.11	99.99
3	99.30	99.99
4	99.06	99.99
5	99.02	99.96
6	99.49	99.99
7	99.40	99.98
8	99.35	99.96
9	99.39	99.96
10	99.28	99.96
<b>Mean</b>	<b>99.25</b>	<b>99.97</b>

Table 11: Test results for relative density

## 9.3 Tensile properties

To compare the mechanical properties between Metal SLS and LPBF, flat tensile specimens were printed according to DIN 50125 Form E [Deu16] with a specimen thickness of  $a_0 = 2$  mm. The results are additionally compared with literature values of cylindrical tensile specimens according to DIN 50125 Form B [Deu16] in order to minimize the manufacturing-related influences of surface roughness in the as-built condition. Testing the flat tensile specimens was conducted at room temperature using a Zwick/Roell AllroundLine testing machine in accordance with DIN EN ISO 6892-1 [Deu20]. For this, a total of five specimens for each AM process was produced in X/Y-plane (horizontal) and Z-direction (vertical). Based on these specimens, the following values were determined:

- Yield strength  $R_{p0.2}$  [N/mm<sup>2</sup>]
- Tensile strength  $R_m$  [N/mm<sup>2</sup>]
- Elongation at break A [%]

The results from the tensile tests are shown in Table 12 and Table 13. From the measurement results, it can be seen that Metal SLS basically exhibits a more ductile material behavior than the LPBF reference. So the elongation at break of Metal SLS (62 %) to LPBF (34 %) is reduced by a maximum of almost half (45.16 %). Similarly, the onset of plastic behavior starts at a significantly lower stress, which differs by 225.48 % from the LPBF reference.

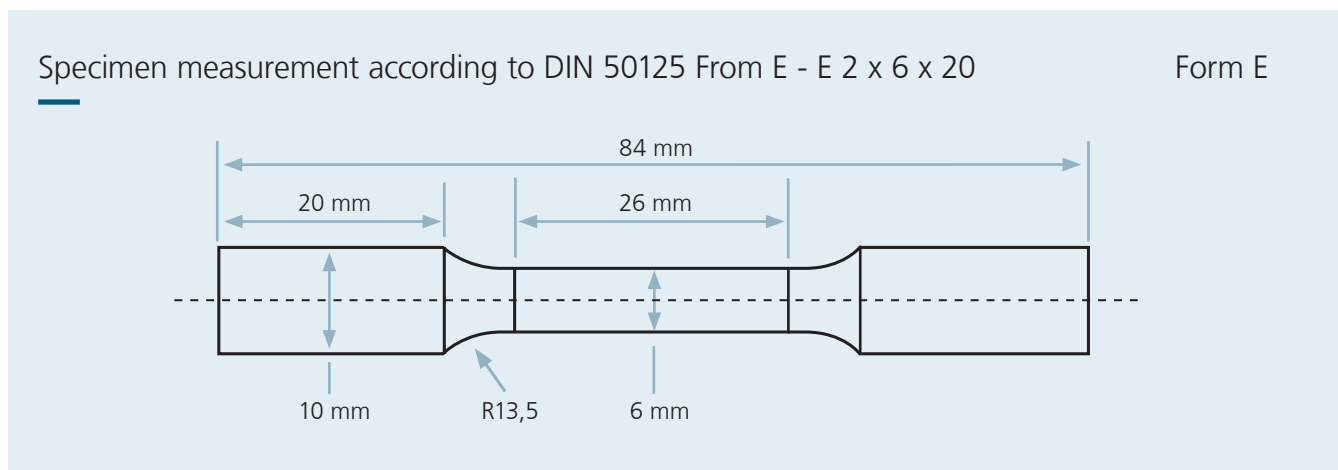


Figure 23: Used tensile specimen form E [Deu16]

Horizontal	$R_{p0.2}$ [MPa]	$R_m$ [MPa]	A [%]
Metal SLS	157	509	62
LPBF	511	641	34
<b>Deviation</b>	<b>225.48 %</b>	<b>25.93 %</b>	<b>45.16 %</b>

Horizontal	$R_{p0.2}$ [MPa]	$R_m$ [MPa]	A [%]
Metal SLS*	201	545	57
LPBF*	555	670	40
<b>Deviation</b>	<b>176.12 %</b>	<b>22.94 %</b>	<b>29.82 %</b>

Table 12: Average values of the tested tensile specimens for Metal SLS and LPBF in horizontal and vertical orientation (including literature values\* [BKW22, SLM23])

A comparison with literature values for cylindrical tensile specimens shows a similar trend. Thus, the percentage deviations for yield strength and elongation at break are of a similar order, 176.12 % and 29.82 %, respectively. For the vertical Metal SLS tensile specimens, the transition from elastic to plastic behavior also begins at a much lower stress compared to LPBF. However, the elongation at break is significantly lower than the horizontal specimens and even lower than the tested LPBF specimens. The literature values, in turn, show a similar trend as before for the horizontal specimens. Furthermore, the tensile strength values determined at Fraunhofer IAPT and the literature values are very close to each other, with the former always being lower. This applies to both the horizontal and

vertical specimens, with the former always being higher. The overall higher ductility of the Metal SLS specimens in horizontal orientation can be illustrated by Figure 25. The reason for this is most likely the coarser structure of Metal SLS specimens in combination with the residual stresses in the LPBF specimens, since all specimens were tested in as-built condition. Likewise, in Figure 25 and Figure 26, it can be seen that the tensile strength is always lower, which could also be attributed to the higher porosity. The earlier failure of the vertical specimens, on the other hand, could be explained by either surface defects (that is probably why the values for cylindrical specimens are higher) or layer bonding defects in form of porosity which are perpendicular to the tensile direction.

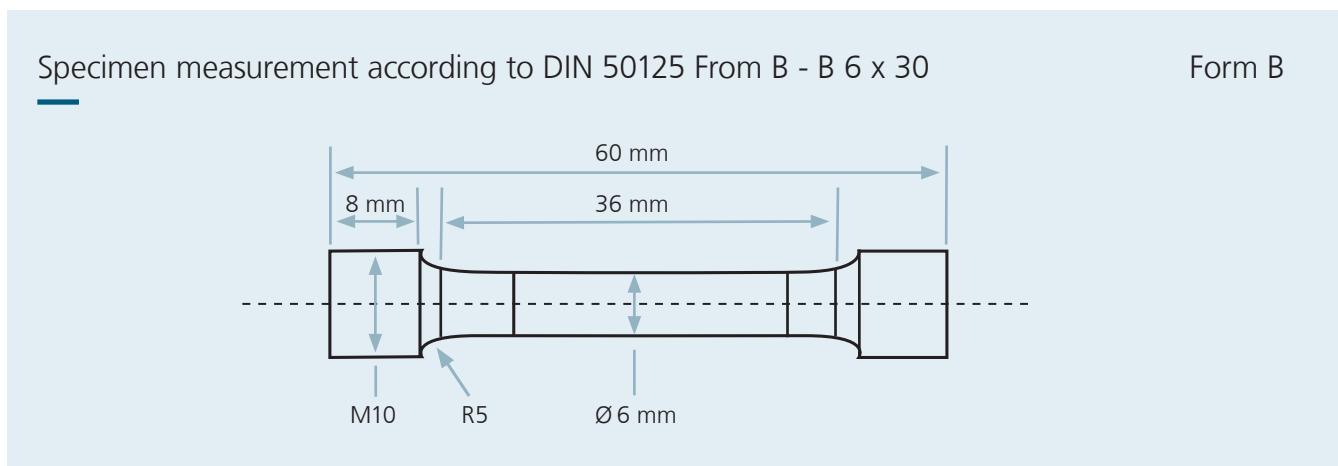


Figure 24: Used tensile specimen form B [Deu16]

Vertical	$R_{p0.2}$ [MPa]	$R_m$ [MPa]	A [%]
Metal SLS	151	449	36
LPBF	441	557	50
<b>Deviation</b>	<b>24.05 %</b>	<b>192.05 %</b>	<b>38.89 %</b>

Vertical	$R_{p0.2}$ [MPa]	$R_m$ [MPa]	A [%]
Metal SLS*	198	536	55
LPBF*	495	615	44
<b>Deviation</b>	<b>150 %</b>	<b>14.74 %</b>	<b>20 %</b>

Table 13: Average values of the tested tensile specimens for Metal SLS and LPBF in horizontal and vertical orientation (including literature values\* [BKW22, SLM23])

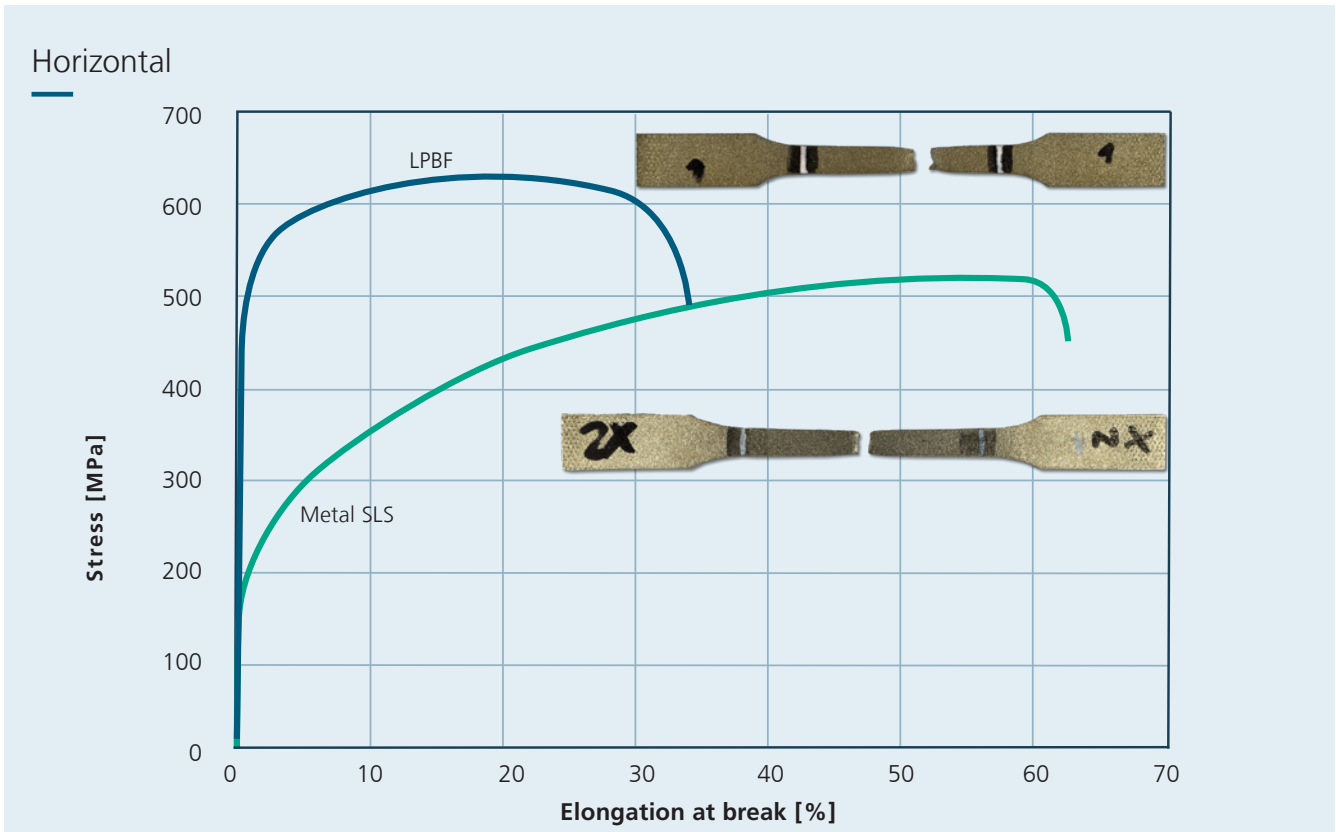


Figure 25: Static tensile strength comparison between Metal SLS and LPBF – Horizontal

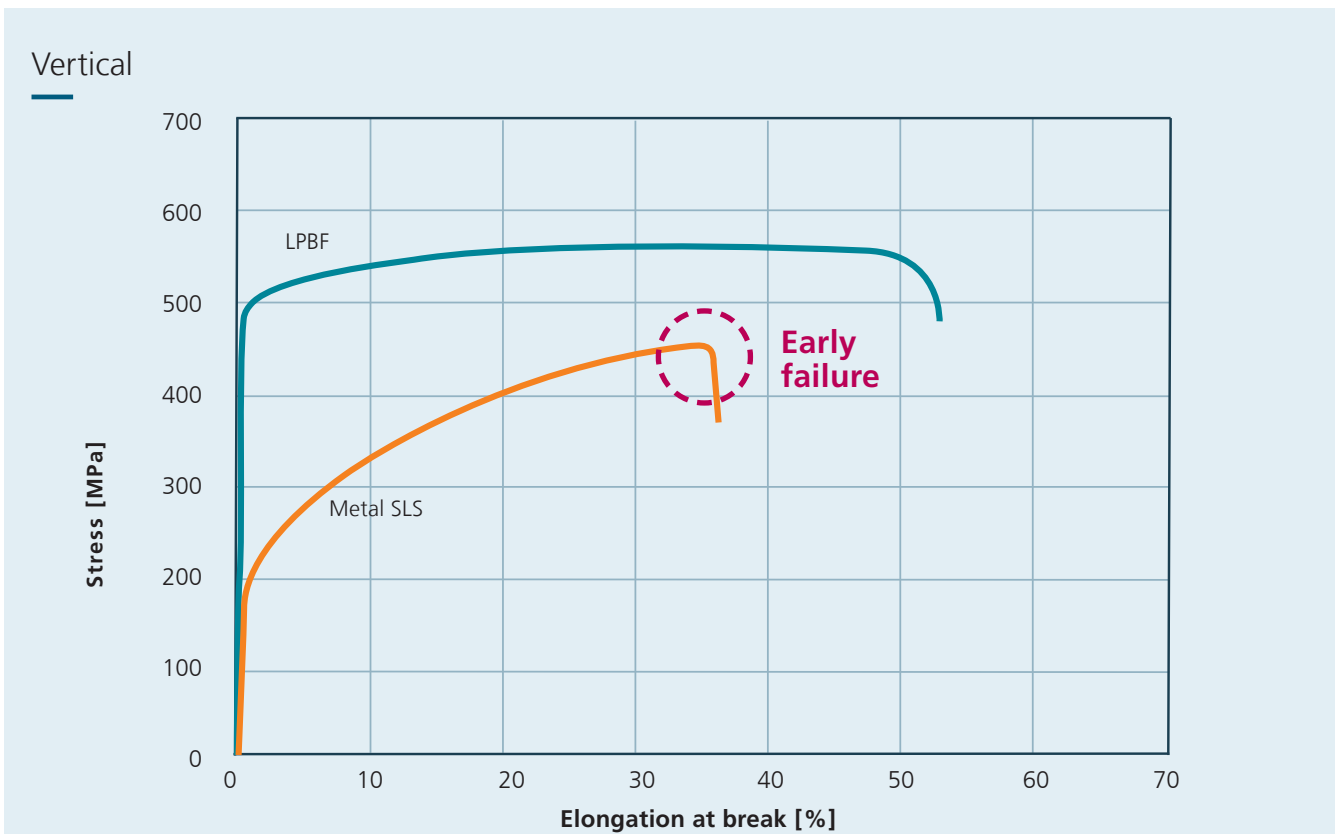


Figure 26: Static tensile strength comparison between Metal SLS and LPBF – Vertical



## 9.4 Vickers hardness

In addition to tensile properties, Vickers hardness was tested to evaluate mechanical properties. According to the Vickers hardness test protocol, a pyramid-shaped diamond was used, which was pressed into the specimen surface with a DuraScan-70 from Struers. The measurement procedure is based on DIN EN ISO 6507-1 [Deu18]. The specimens used for the density measurement were grinded and polished in preparation and then evaluated according to test method HV10. The square diamond indenter was pressed into the material at a pyramid angle of  $136^\circ$  with a controlled force of 10 kg (98 N). Figure 27 shows the example of a hardness measuring point whose indentation was repeated at 8 other points on the specimen surface.

The mean hardness (HV10) of the Metal SLS specimens is 118 and for LPBF 218, as can be seen in Table 14. The results thus confirm the more ductile behavior of the Metal SLS specimens observed previously. On average, the hardness values differ by 100 HV10 (84.75 %).

### Vickers hardness measurements

Cube No.	Vickers hardness [HV10]	
	Metal SLS	LPBF
1	117	217
2	117	218
3	116	219
4	118	218
5	117	221
6	118	218
7	120	217
8	118	219
9	118	217
<b>Mean</b>	<b>118</b>	<b>218</b>

Table 14: Results for Vickers hardness measurement

### Measurement setup

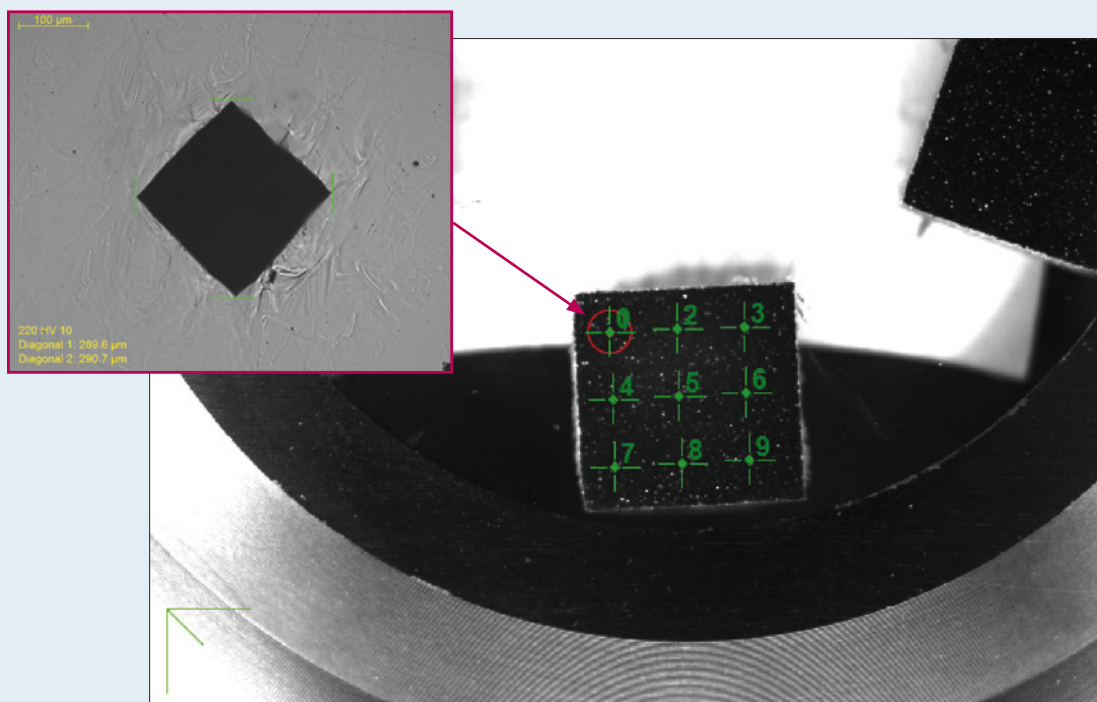


Figure 27: Hardness measuring point and measurement setup

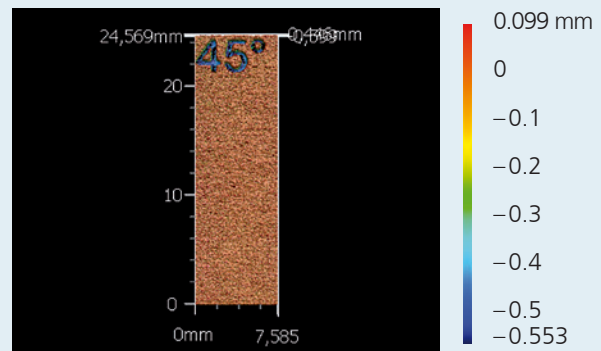
## 9.5 Surface quality

In the context of surface roughness analysis, a series of test specimens were fabricated that had different angles of inclination to the build platform, as illustrated in Figure 28. The roughness properties were obtained according to DIN EN ISO 21920-2 [Deu22] in which 8 mm long lines on the specimens surface were scanned using a stripe light microscope with a resolution of 0.1  $\mu\text{m}$ .

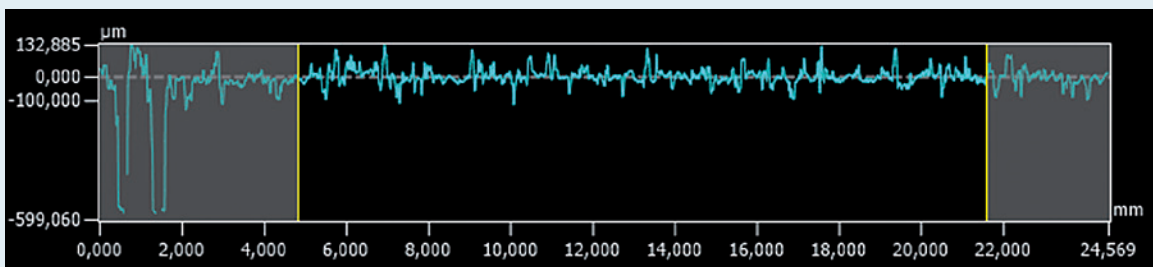
The central focus of this investigation was an effort to quantify roughness average and roughness depth in the context of the Metal SLS and LPBF manufacturing processes. It should be

emphasized here that the parameters used were not explicitly designed to optimize surface properties. A productivity-optimized surface parameter set was used to fabricate the LPBF specimens. However, this was accompanied by a slight compromise in surface quality compared to a parameter set focused exclusively on surface optimization. Nevertheless, the use of this LPBF parameter set reflects a good suitability for the production of economical part fabrication with a demand for surface quality, which is well suited for Metal SLS comparison.

### Surface roughness Metal SLS and LPBF



Overall profile



Roughness profile

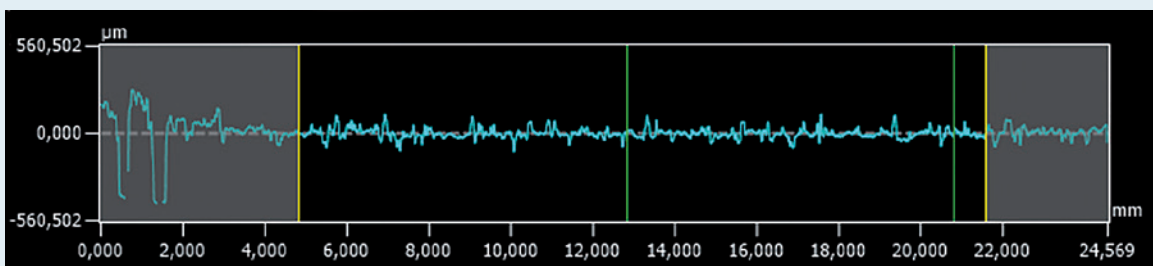


Figure 28: Exemplary measurement of the 45° surface on a LPBF specimen

The comparison between the processes in Table 15 shows that the surface quality in terms of Ra and Rz exhibited by the LPBF specimens are, on average, slightly higher than those of the Metal SLS surfaces. For angled surfaces, the staircase effect additionally comes into play, which has a stronger negative influence on the surface quality with higher layer thickness (Metal SLS: 100  $\mu\text{m}$ , LPBF: 40  $\mu\text{m}$ ). However, the differences between the tested angles are not particularly strong (Metal SLS: max. 2.27  $\mu\text{m}$ , LPBF: max. 1.18  $\mu\text{m}$ ), as can be seen in Table 15.

It should be noted that possibilities for increasing the surface quality are revealed by means of subsequent postprocessing processes, such as the application of techniques like sandblasting or electropolishing. For LPBF, this postprocessing always takes place on the finished metal part. For Metal SLS, there is the additional option of mechanically postprocessing the green parts that have not yet been sintered, which saves time and costs.

### Surface roughness Metal SLS and LPBF

Process	Orientation [°]	Ra [ $\mu\text{m}$ ]	Rz [ $\mu\text{m}$ ]
Metal SLS	0	32.19	246.16
	15	53.33	335.07
	30	50.15	314.14
	45	52.49	337.90
	60	52.87	321.23
	90	41.67	275.90

Process	Orientation [°]	Ra [ $\mu\text{m}$ ]	Rz [ $\mu\text{m}$ ]
LPBF	0	13.80	147.75
	15	23.32	228.97
	30	16.77	182.50
	45	15.63	180.16
	60	16.81	188.13
	90	13.01	155.57

Table 15: Results of the surface analysis for the Metal SLS and LPBF in as-built condition

# 10. Summary & Conclusion

A summary of the results from the economic and quality comparison is provided in Table 16. It is clear that Metal SLS is significantly more economical for the use case considered. LPBF, on the other hand, is convincing in terms of part quality, which is always better than Metal SLS except for ductility. The quality of Metal SLS parts could be improved by subsequent processes such as further heat treatment (e.g. HIP) or prior green part finishing. However, this is again at the expense of costs per unit and lead time and must therefore be decided depending on the application. In addition, process

optimizations in printing and sintering also offer room for bringing part quality more into line with LPBF.

Ultimately, it remains to be said that Metal SLS can certainly be a cost- and material-efficient alternative for LPBF. This is especially true for MIM users. These can integrate Metal SLS as a complementary AM production technology in order to produce quantities that are uneconomical for MIM. The existing debinding and sintering system technology can be utilized, offering major cost advantages.

## Final comparison



















Investigated Properties		Metal SLS		LPBF	
Economical comparison	 Costs per unit (n = 1000)	Base: 10.09 € Big furnace: 8.93 €		Base: 33.29 € Four lasers: 40.41 €	
	 Lead time (n = 1000)	Base: 314 h Big furnace: 287 h		Base: 742 h Four lasers: 675 h	
	 Material efficiency	Max. 2 % powder loss (vacuuming)		Max. 11.2 % powder loss + supports	
Quality comparison	 Dimensional accuracy	X = - 1.79 % Y = - 1.18 % Z = + 0.17 %		X = - 0.90 % Y = - 0.94 % Z = + 0.51 %	
	 Density	$\rho = 99.25 \%$		$\rho = 99.97 \%$	
	 Tensile strength	$R_{mXY} = 509 \text{ MPa}$ $R_{mZ} = 449 \text{ MPa}$		$R_{mXY} = 641 \text{ MPa}$ $R_{mZ} = 557 \text{ MPa}$	
	 Ductility	$A_{XY} = 62 \%$ ( $A_Z = 36 \%$ )		$A_{XY} = 34 \%$ ( $A_Z = 50 \%$ )	
	 Vickers hardness	118 HV10		218 HV10	
	 Surface quality	$R_a = 47.12 \mu\text{m}$ $R_z = 305.07 \mu\text{m}$		$R_a = 16.56 \mu\text{m}$ $R_z = 180.51 \mu\text{m}$	

Table 16: Intended summary of the results obtained



# 11. References

---

- [Deu16] Deutsches Institut für Normung e.V., „Prüfung metallischer Werkstoffe – Zugproben, 50125:2016-12“, Berlin, Dec. 2016. [Online] Available: <https://www.beuth.de/de/norm/din-50125/262241217>
- [Deu18] Deutsches Institut für Normung e.V., „Metallische Werkstoffe – Härteprüfung nach Vickers Teil 1: Prüfverfahren“, 6507-1:2018-07, Berlin, Jul. 2018. [Online] Available: <https://www.beuth.de/de/norm/din-en-iso-6507-1/280959455>
- [Deu20] Deutsches Institut für Normung e.V., „Metallische Werkstoffe – Zugversuch - Teil 1: Prüfverfahren bei Raumtemperatur, 6892-1:2020-06“, Berlin, Jun. 2020.
- [Deu22] Deutsches Institut für Normung e.V., „Geometrische Produktspezifikation (GPS) - Oberflächenbeschaffenheit: Profile – Teil 2: Begriffe und Kenngrößen für die Oberflächenbeschaffenheit, 21920-2:2022-12“, Berlin, Dec. 2022.
- [BKW22] BK Werkstofftechnik – Prüfstelle für Werkstoffe GmbH, „Prüfbericht Headmade 316L nach DIN EN ISO 17025,“, Email, Jan. 2022.
- [Hea20] Headmade Materials GmbH, „Cold Metal Fusion/ Metal SLS – Technology“ Unterpleichfeld, Oct 2020.
- [Hea22] Headmade Materials GmbH, „Stainless Steel 316L: Edelstahl 316L.“ <https://www.headmade-materials.de/files/content/downloads/material-datasheets/material-datasheet-stainless-steel-316l-a5.pdf> (accessed Aug. 25, 2023).
- [Hea22a] Headmade Materials GmbH, „Stainless Steel 316L: Edelstahl 316L.“, [Online] Available: <https://www.headmade-materials.de/files/content/downloads/material-datasheets/material-datasheet-stainless-steel-316l-a5.pdf> (accessed Aug. 25, 2023).
- [Hea22b] Headmade Materials GmbH, „Guideline to design parts: Cold metal fusion.“, Email, 26.04.2023.
- [Jul23] JULIAN REEH, „SEM-image of 316L feedstock from Headmade Materials“, E-Mail, Aug. 2023.
- [Sch15] SCHMID, F., „Selektives Lasersintern (SLS) mit Kunststoffen“ Carl Hanser Verlag, München, 2015.
- [SLM23] SLM Solutions Group AG, „Material Data Sheet 316L: ASTM A276 / DIN EN 10088 / 1.4404,“, [Online] Available: [https://www.slm-solutions.com/fileadmin/Content/Powder/MDS/nw/MDS\\_316L\\_2023-04\\_EN.pdf](https://www.slm-solutions.com/fileadmin/Content/Powder/MDS/nw/MDS_316L_2023-04_EN.pdf) (accessed Sep. 1, 2023).
- [Thy23] Thyssen Krupp Materials Trading GmbH, „Material data sheet 1.4404“, Essen, 2023.

## Imprint

---

**Fraunhofer Research Institution for  
Additive Manufacturing Technologies IAPT**  
Am Schleusengraben 14  
21029 Hamburg-Bergedorf  
Germany

Telephone +49 40 48 40 10-500  
[www.iapt.fraunhofer.de](http://www.iapt.fraunhofer.de)  
[marketing@iapt.fraunhofer.de](mailto:marketing@iapt.fraunhofer.de)

A legally dependent entity of  
**Fraunhofer-Gesellschaft zur Förderung  
der angewandten Forschung e.V.**  
Hansastraße 27c  
80686 Munich  
Germany  
[www.fraunhofer.de](http://www.fraunhofer.de)  
[info@zv.fraunhofer.de](mailto:info@zv.fraunhofer.de)

Status of the Deep Dive, October 2023

## Contact

---

Christian Böhm, M. Sc.  
Head of Additive Alliance®  
Telephone +49 40 48 40 10-636  
eMail [christian.boehm@iapt.fraunhofer.de](mailto:christian.boehm@iapt.fraunhofer.de)

The Fraunhofer IAPT does not warrant that the information in this Deep Dive is correct. No statement in this Deep Dive shall be considered as an assured prediction. The reader should not make any decision based exclusively on the information presented.

Photo credits:  
all image rights are held by Fraunhofer IAPT.

Copyright | All rights reserved.  
No reproduction or distribution of this document without the expressed consent of Fraunhofer IAPT.

